AD-A078 003 GEORGIA INST OF TECH ATLANTA ENGINEERING EXPERIMENT --ETC F/G 7/4
SUBMILLIMETER WAVE SPECTROSCOPY AND TECHNOLOGY.(U)
OCT 79 J J GALLAGHER DAAG29-76-G-0280

UNCLASSIFIED ARO-14104.5-PX NL

| OF |
AD
A078003

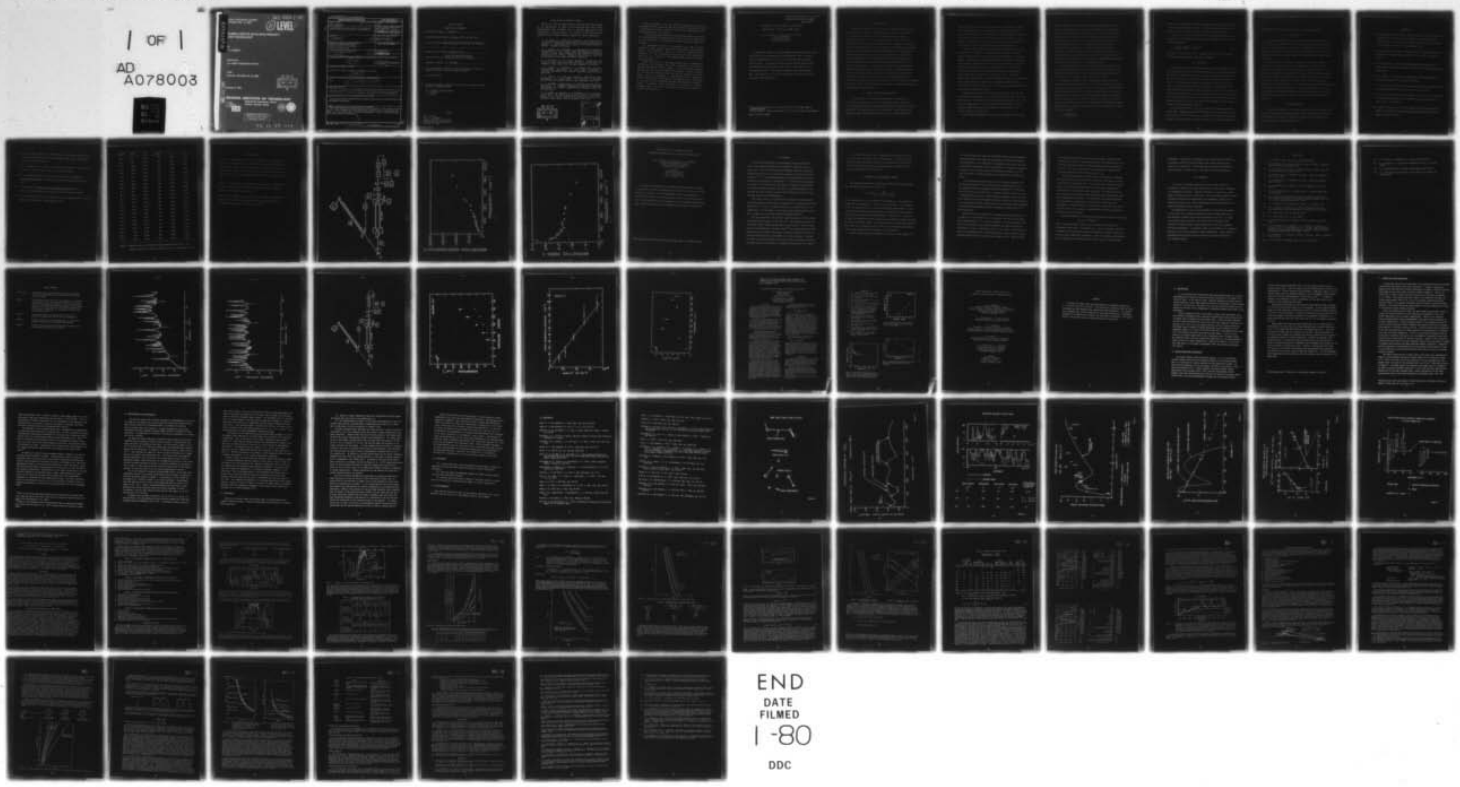

END
DATE
FILMED
1-80
DDC

ARO 14104.5-PX

LEVEL II

FINAL TECHNICAL REPORT
PROJECT NO. A–1861

SUBMILLIMETER WAVE SPECTROSCOPY AND TECHNOLOGY

by
J. J. Gallagher

Prepared for
U.S. ARMY RESEARCH OFFICE

Under
Grant No. DAAG29–76–G–0280

October 8, 1979

GEORGIA INSTITUTE OF TECHNOLOGY
Engineering Experiment Station
Atlanta, Georgia 30332

GTEES

1979

Unclassified

SECURITY CLASSIFICATION OF THIS PAGE (When Data Entered)

REPORT DOCUMENTATION PAGE

READ INSTRUCTIONS BEFORE COMPLETING FORM

1. REPORT NUMBER: FINAL TECHNICAL	2. GOVT ACCESSION NO.
3. RECIPIENT'S CATALOG NUMBER: (9)	
4. TITLE (and Subtitle): (6) SUBMILLIMETER WAVE SPECTROSCOPY AND TECHNOLOGY,	5. TYPE OF REPORT & PERIOD COVERED: FINAL TECHNICAL Rept. 1 January — 30 June, 1979
	6. PERFORMING ORG. REPORT NUMBER
7. AUTHOR(s): (10) J. J. Gallagher	8. CONTRACT OR GRANT NUMBER(s): (15) DAAG29-76-G-0280
9. PERFORMING ORGANIZATION NAME AND ADDRESS: Engineering Experiment Station, Georgia Institute of Technology, Atlanta, Georgia 30332 ✓	10. PROGRAM ELEMENT, PROJECT, TASK AREA & WORK UNIT NUMBERS
11. CONTROLLING OFFICE NAME AND ADDRESS: U. S. Army Research Office, P. O. Box 12211, Research Triangle Park, NC 27709 (11) 8	12. REPORT DATE: October 8, 1979
	13. NUMBER OF PAGES
14. MONITORING AGENCY NAME & ADDRESS (if different from Controlling Office): (12) 74	15. SECURITY CLASS. (of this report): Unclassified
	15a. DECLASSIFICATION/DOWNGRADING SCHEDULE: N/A

16. DISTRIBUTION STATEMENT (of this Report)

Approved for public release; distribution unlimited.

(18) ARO

17. DISTRIBUTION STATEMENT (of the abstract entered in Block 20, if different from Report)

N/A (19) 1412 4.5-PX

18. SUPPLEMENTARY NOTES

The view, opinions, and/or findings contained in this report are those of the author(s) and should not be construed as an official Department of the Army position, policy, or decision, unless so designated by other documentation.

19. KEY WORDS (Continue on reverse side if necessary and identify by block number)

Submillimeter Waves; Schottky Barrier Diodes; Spectroscopy; Heterodyne Receivers; Atmospheric Absorption.

20. ABSTRACT (Continue on reverse side if necessary and identify by block number)

The investigations performed during the final 6-months of the program are described. These included optically-pumped laser spectroscopy of liquid water and water vapor and submillimeter receiver investigations. Papers on work performed during this period are attached.

DD FORM 1 JAN 73 1473 EDITION OF 1 NOV 65 IS OBSOLETE

Unclassified

SECURITY CLASSIFICATION OF THIS PAGE (When Data Entered)

153850

PROGRESS REPORT

(TWENTY COPIES REQUIRED)

1. ARO PROPOSAL NUMBER: P-14104-PX

2. PERIOD COVERED BY REPORT: 31 January, 1979 - 30 June, 1979

3. TITLE OF PROPOSAL: SUBMILLIMETER WAVE SPECTROSCOPY AND TECHNOLOGY

4. CONTRACT OR GRANT NUMBER: DAAG29-76-G-0280

5. NAME OF INSTITUTION: Engineering Experiment Station
Georgia Institute of Technology

6. AUTHOR(S) OF REPORT: J. J. Gallagher

7. LIST OF MANUSCRIPTS SUBMITTED OR PUBLISHED UNDER ARO SPONSORSHIP DURING THIS PERIOD, INCLUDING JOURNAL REFERENCES:

See attached sheet.

8. SCIENTIFIC PERSONNEL SUPPORTED BY THIS PROJECT AND DEGREES AWARDED DURING THIS REPORTING PERIOD:

O. A. Simpson, Graduate Student
J. J. Gallagher
W. Fife

14104-P

Dr. M. D. Blue
Dr. J. J. Gallagher
Georgia Institute of Technology
Engineering Experiment Station
Atlanta, GA 30332

BRIEF OUTLINE OF RESEARCH FINDINGS

During the last six month period of the Grant, work was performed on the spectroscopy of water in both liquid and vapor state. These investigations were performed with an optically pumped laser as the submillimeter radiation source. The details of this work have been presented in the following Conference papers and journal submissions:

1. O. A. Simpson, B. L. Bean and S. Perkowitz, "Far Infrared Optical Constants of Liquid Water Measured With An Optically Pumped Laser," accepted for publication in the Journal of the Optical Society of America - December, 1979 issue.

2. O. A. Simpson, R. A. Bohlander, J. J. Gallagher and S. Perkowitz, "Measurements of Far Infrared Water Vapor Between Lines With An Optically Pumped Laser," presented at The Conference on Microwave Spectroscopy and Coherent Radiation, Duke University, June, 1979 and submitted to the Journal of Physical Chemistry.

3. R. A. Bohlander et al, "Excess Absorption by Water Vapor and Comparison With Theoretical Dimer Absorption," Proceedings of the Workshop on Water Vapor, Vail, Colorado, September 11-13, 1979.

4. O. A. Simpson, R. A. Bohlander, J. J. Gallagher and S. Perkowitz, "Submillimeter Spectroscopy of Water Vapor," Conference on Microwave Spectroscopy and Coherent Radiation, Duke University, June, 1979.

5. O. A. Simpson, B. L. Bean and S. Perkowitz, "Submillimeter Laser Spectroscopy of Liquid Water," The Conference on Microwave Spectroscopy and Coherent Radiation, Duke University, June, 1979.

6. J. J. Gallagher, "Applications of Millimeter and Submillimeter Spectroscopy to Atmospheric Propagation," Conference on Microwave Spectroscopy and Coherent Radiation, Duke University, June, 1979 (Invited Paper).

7. O. A. Simpson, S. Perkowitz, R. A. Bohlander and J. J. Gallagher, "Far-Infrared Laser Spectroscopy of Water Vapor and Liquid Water," Digest of the Fourth International Conference on Infrared and Millimeter Waves, Miami, Florida, December 10-15, 1979.

These measurements with the optically pumped laser are the initial measurements of this nature and will be extended to obtain detailed data on atmospheric absorption. The work is part of the requirements for the doctorate degree of O. A. Simpson.

A quasi-optical diplexer and bi-conical Schottky barrier mixer have been constructed and are undergoing tests with an optically pumped laser as local oscillator. This work will be reported when final results are obtained.

Two manuscripts currently in preparation have been partially supported by ARO. Copies of these will be forwarded to the ARO Physics Division upon completion. They are a paper on Submillimeter Wave Techniques, for the Proceedings of the IEEE, and one on Quasi-Optics, which will be a chapter in the Academic Press series on Millimeter through IR Physics.

During the course of this program, many topics on submillimeter spectroscopy and techniques have been investigated and reported in previous semi-annual reports. Many of these topics have potential applications in the area of NMMW military systems. A paper, presented at the 1979 IRIS Conference and at the 1979 SPIE Conference as invited papers, shows the importance of spectroscopy related to atmospheric effects and research on technology in this spectral region. This paper is a result of partial support by HDL under ARO Contract No. DAAG29-77-C-0026. A technical report presenting an overview of the research performed under this grant is in preparation and will be submitted to the ARO Physics Division.

ACCEPTED FOR PUBLICATION IN THE JOURNAL
OF THE OPTICAL SOCIETY OF AMERICA
FINAL VERSION

FAR INFRARED OPTICAL CONSTANTS OF LIQUID WATER MEASURED WITH AN OPTICALLY PUMPED LASER*

O. A. Simpson, B. L. Bean,† and S. Perkowitz
Physics Department
Emory University
Atlanta, Georgia 30322

A tunable far infrared optically pumped laser has been used to measure the reflection R and transmission of liquid water at 25°C. The laser covered the range 8.22 to 175.7 cm^{-1} with an average spacing between lines of 8 cm^{-1}. The optical data were used to find the complex index of refraction n-ik with typical errors of 2%. A small peak in n was observed near 55 cm^{-1}. This feature correlates with published Raman data. The values of R, n, k and the absorption coefficient α are given in graphical and tabular form.

*Work partially supported by the Army Research Office under Grant No. DAAG29-76-G-0280.
†Present address: Science Applications Inc., Drawer E, White Sands Missile Range, New Mexico 88002.

I. INTRODUCTION

Liquid water absorbs so heavily in the far infrared (FIR) range that it is difficult to accurately measure its transmission. Many workers have determined the complex index of refraction n-ik with varying degrees of precision.[1] Afsar and Hasted (AH) have avoided the absorption problem by using reflection dispersive Fourier transform spectroscopy. They first measured n-ik at a water temperature of 19°C[2] and later accurately found n-ik at 4, 30, and 57°C.[3] An alternate method is to directly measure the transmission through a sizable water pathlength with a high power optically pumped FIR laser. Since free surface reflection measurements are also feasible with a laser, FIR laser spectroscopy gives n-ik in an elegantly simple manner. In this paper we present laser results between 8.22 and 175.7 cm^{-1} at a water temperature of 25°C. Our data are superior to the previously reported results at this temperature,[4] provide better low frequency coverage than was available to AH, and give evidence for a temperature dependent low frequency feature near 55 cm^{-1}. The general agreement between the results of AH and our data is so good as to confirm the validity of both experimental techniques.

II. EXPERIMENTAL METHODS AND RESULTS

A block diagram of the experimental apparatus is shown in Fig. 1. A 25 W CO_2 laser drives a FIR laser of the waveguide type. Details of this laser spectrometer (and early water measurements) have been previously reported,[5,6] but some improvements have been made. A new CO_2 laser was constructed with a PZT mounted ZnSe mirror to allow tuning of the line

center frequency to match the absorption transition frequency. Sampling of the FIR beam (signal I_s) by the pyroelectric detector D_1 allowed the CO_2 laser to be frequency stabilized so as to keep the FIR power constant. This helped to eliminate amplitude fluctuations in the FIR laser output caused by instabilities in the CO_2 laser. An opto-acoustic detector[7] on the FIR cavity aided in tuning difficult absorption transitions.

The main signal entered the Fabry-Perot interferometer (FP) which was used both to measure the wavelength and as a filter to eliminate unwanted wavelengths that may have lased simultaneously with the desired signal. The FIR beam was then divided by BS_2. The reference signal I_B, after detection and amplification by a Golay cell and lock-in amplifier, entered the denominator channel of the ratiometer RA. The signal I_A was, as will be described, reflected from or transmitted through the water sample and then detected by another Golay cell. This signal, after lock-in amplification, became the numerator signal in the ratiometer. This ratioing process was important in eliminating additional source fluctuations in the FIR power level. Values of I_A/I_B from the ratiometer were the basic experimental signal.

Although there are hundreds of optically pumped FIR lines arising from dozens of pumped media, it is simplest to work with only a few media when possible. We obtained 23 FIR lines between 8.22 and 175.7 cm^{-1} using only four pumped gases as has been fully described elsewhere.[8] This frequency range and coverage is comparable to that available to AH in their dispersive Fourier work.

Free surface measurements of the reflection coefficient R were made

on distilled water at 25±1°C. A mirror deflected the FIR beam to near-normal incidence with the horizontal water surface and a second mirror directed the reflected beam into the detector. The 7.5° incident angle was small enough that the assumption of normal incidence introduced a negligible error. In addition, the FIR radiation was unpolarized which further decreased this error. The water was placed in a container several mm deep, so that the back surface reflection was totally negligible. The water container could be replaced when desired with a standard reflector, a gold coated mirror of 99 ± 1% reflectivity. The coincidence of the water and mirror surfaces on interchange was constantly monitored by the reflection of a fixed HeNe laser beam.

For each FIR frequency several values of I_A/I_B were determined for reflection from the water surface and reflection from the standard mirror. The ratio of the two values of I_A/I_B then yielded R with typical random errors under 1%. The measured values are given in Table I.

An adjustable pathlength cell with crystalline quartz windows was used in the transmission measurements. The cell was mounted on a translation stage-fixed stage arrangement with a high accuracy (0.002 mm/division) micrometer head screw drive. A dial gauge, attached directly to the cell housing, gave a second determination of pathlength changes for comparison with the micrometer drive. Values of I_A/I_B were measured at increments of 5μm to an accuracy of 1μm over an average change in pathlength of 60μm. These data made it possible to determine the Lambert absorption coefficient α from the relation[9]

$$\alpha = -\frac{\Delta[\ell n(I_A/I_B)]}{\Delta x} \qquad (1)$$

where x is the pathlength. An error weighted least squares fit was applied to the data at each laser frequency f to determine $\alpha(f)$ and the associated error, typically 2%. The resulting values of α are shown in Fig. 2.

Values of $k = \alpha/4\pi f$ were calculated from the measured absorptions and together with the appropriate R, were used to determine n from the normal incidence expression:

$$n = \frac{1 + R}{1 - R} + \left[\left(\frac{1+R}{1-R}\right)^2 - (k^2+1)\right]^{1/2} \qquad (2)$$

The results are plotted in Fig. 3. Numerical values of all the measured and derived optical quantities are given in Table I.

III. DISCUSSION

Our data at 25°C are in excellent agreement with those of AH[3] at 30°C. Other published data near 25°C disagree strongly with these combined results. The 19°C values AH[2] found for n are well below the present data between 50 and 150 cm^{-1} and even lie below their own later 4°C data between 70 and 150 cm^{-1}. The Downing and Williams[1] values for n at 27°C, on the other hand, are significantly greater than the present results above 100 cm^{-1}. These conflicting observations could be reconciled only if the FIR properties of water show radical and non-monotonic temperature dependences between 4 and 30°C. This possibility remains to be explored, but the good agreement between the present data at 25°C and the AH data at 30°C suggests that the results at 19 and 27°C are experimental anomalies.

An interesting feature of the laser results is the small maximum in n near 55 cm^{-1}. Raman measurements[10,11,12] have shown the presence of a small peak near 60 cm^{-1} at 25°C but earlier FIR data[4] do not exhibit this feature because of the relatively poor signal-to-noise ratio. The peak magnitude is

clearly greater than the ranlom error in our measurements, however.

IV. CONCLUSIONS

Our laser measurements of n and k at 25°C are in excellent agreement with the 30°C reflection dispersive Fourier data of Afsar and Hasted. The random errors in the measurements are comparable. Assuming that there is no strong temperature dependence in the general optical properties of water in this temperature range, the agreement attests to the validity of both experimental techniques.

Our data exhibit a low frequency peak near 55 cm^{-1} which appears to correlate with similar structure seen in Raman data. The Raman peak is believed to arise from hydrogen bond stretching and bending motions.[10] We have begun to examine the peak behavior by making multi-oscillator, relaxation model, and Kramers-Kronig analyses of our highly accurate reflectivity data. Preliminary results suggest that relaxation rather than resonant effects dominate in this frequency region. This analysis is continuing and we plan also to study the position and amplitude of the peak *vs* temperature. The laser spectrometer will be used for further accurate measurements as a function of temperature, with potential for shedding light on basic molecular processes in water.

V. ACKNOWLEDGEMENTS

The authors are grateful to Professor Dudley Williams for suggesting the laser surface reflection measurements and for his encouragement of the work. We also thank M. N. Afsar for providing a preprint of the recent work at 4, 30 and 57°C and for his helpful discussions.

REFERENCES

1. Thorough reviews of FIR work in water are given by P. S. Ray, "Broadband Complex Refractive Indices of Ice and Water," Appl. Opt. 11, 1836 (1972); and H. O. Downing and D. Williams, "Optical Constants of Water in the Infrared," J. Geophys. Res. 80, 1656 (1975).

2. M. N. Afsar and J. B. Hasted, "Measurements of the Optical Constants of Liquid H_2O and D_2O between 6 and 450 cm^{-1}," J. Opt. Soc. Am. 67, 902 (1977).

3. M. N. Afsar and J. B. Hasted, "Submillimeter Wave Measurements of Optical Constants of Water at Various Temperatures," Infrared Physics 18, 835 (1978).

4. M. S. Zafar, J. B. Hasted, and J. Chamberlain, "Water-Submillimeter Dielectric Dispersion," Nature 243, 106 (1973).

5. B. L. Bean and S. Perkowitz, "Far-infrared Transmission Measurements with an Optically Pumped FIR Laser," Appl. Opt. 11, 2617 (1976).

6. B. L. Bean and S. Perkowitz, "Submillimeter - Far Infrared Spectroscopy in the Liquid and Solid States with a Tunable Optically Pumped Laser," J. Opt. Soc. Am. 7, 911 (1977).

7. G. Busse, E. Basel, and A. Pfaller, "Application of the Opto-Acoustic Effect to the Operation of Optically Pumped Far-Infrared Gas Lasers," Appl. Phys. 12, 387 (1977).

8. B. L. Bean and S. Perkowitz, "Complete Frequency Coverage for Submillimeter Laser Spectroscopy with Optically Pumped CH_3OH, CH_3OD, CD_3OD, and CH_2CF_2," Optics Letters 1, 202 (1977).

9. D. A. Draegert, N. W. B. Stone, B. Curnutte, and D. Williams," Far Infrared Spectrum of Liquid Water," J. Opt. Soc. Am. 56, 64 (1966).

10. G. E. Walrafen, "Liquid Water: Dielectric Properties," in Water: A Comprehensive Treatise, F. Franks, Ed., (Plenum, New York, 1972), pp. 151-165.

11. G. E. Walrafen in Structure of Water and Aqueous Solutions, W. A. P. Luck, Ed., (Verlag Chemie-Physik Verlag, Weinheim, 1974), pp. 319-320.

12. O. F. Nielsen, "The Structure of Liquid Water; a Low Frequency (10 - 400 cm^{-1}) Raman Study," Chem. Phys. Letters 60, 515 (1979).

f(cm^{-1})	λ(μm)	R	α(cm^{-1})	n	k
8.2	1217	0.297	121	2.857	1.174
11.2	890	0.249	150	2.462	1.062
13.1	764.1	0.228	148	2.437	0.902
14.3	699.5	0.228	171	2.383	0.950
17.5	570.5	0.201	173	2.306	0.784
21.2	471	0.191	199	2.252	0.746
24.0	417	0.185	215	2.231	0.714
24.6	406.4	0.184	206	2.267	0.665
26.8	372.7	0.179	235	2.197	0.696
30.3	330	0.164	228	2.155	0.598
34.2	292.6	0.161	259	2.126	0.604
35.5	281.5	0.155	250	2.112	0.560
39.4	254	0.147	221	2.125	0.447
43.6	229.1	0.144	289	2.050	0.527
52.1	191.7	0.140	285	2.079	0.435
54.5	183.6	0.147	355	2.082	0.519
61.3	163	0.140	339	2.076	0.440
69.1	144.8	0.136	405	2.025	0.466
84.2	118.8	0.134	457	2.034	0.432
98.4	101.6	0.131	605	1.976	0.489
103.6	96.5	0.136	696	1.985	0.534
141.6	70.6	0.122	986	1.845	0.554
175.7	56.9	0.095	1147	1.652	0.519

Table I. Measured values of reflection R and absorption coefficient α, and derived values of the index of refraction n-ik for liquid water at 25°C.

FIGURE CAPTIONS

Figure 1. Block diagram of the FIR laser spectrometer: m, mirrors; G, grating; L, lens; SA, spectrum analyzer; PZT, piezoelectric transducer; C, chopper; D, detectors; BS, beamsplitters; FP, Fabry-Perot interferometer; S, water sample; LI, lock-in amplifier; RA, digital ratiometer; FS, frequency stabilizer; SC, stripchart recorder; OAD, opto-acoustic detector.

Figure 2. Laser results for the absorption coefficient of liquid water at 25°C. The symbols for the laser experimental points are slightly larger than the typical random errors.

Figure 3. Laser results for the real part of the index of refraction of liquid water at 25°C. The symbols for the laser experimental points are slightly larger than the typical random errors.

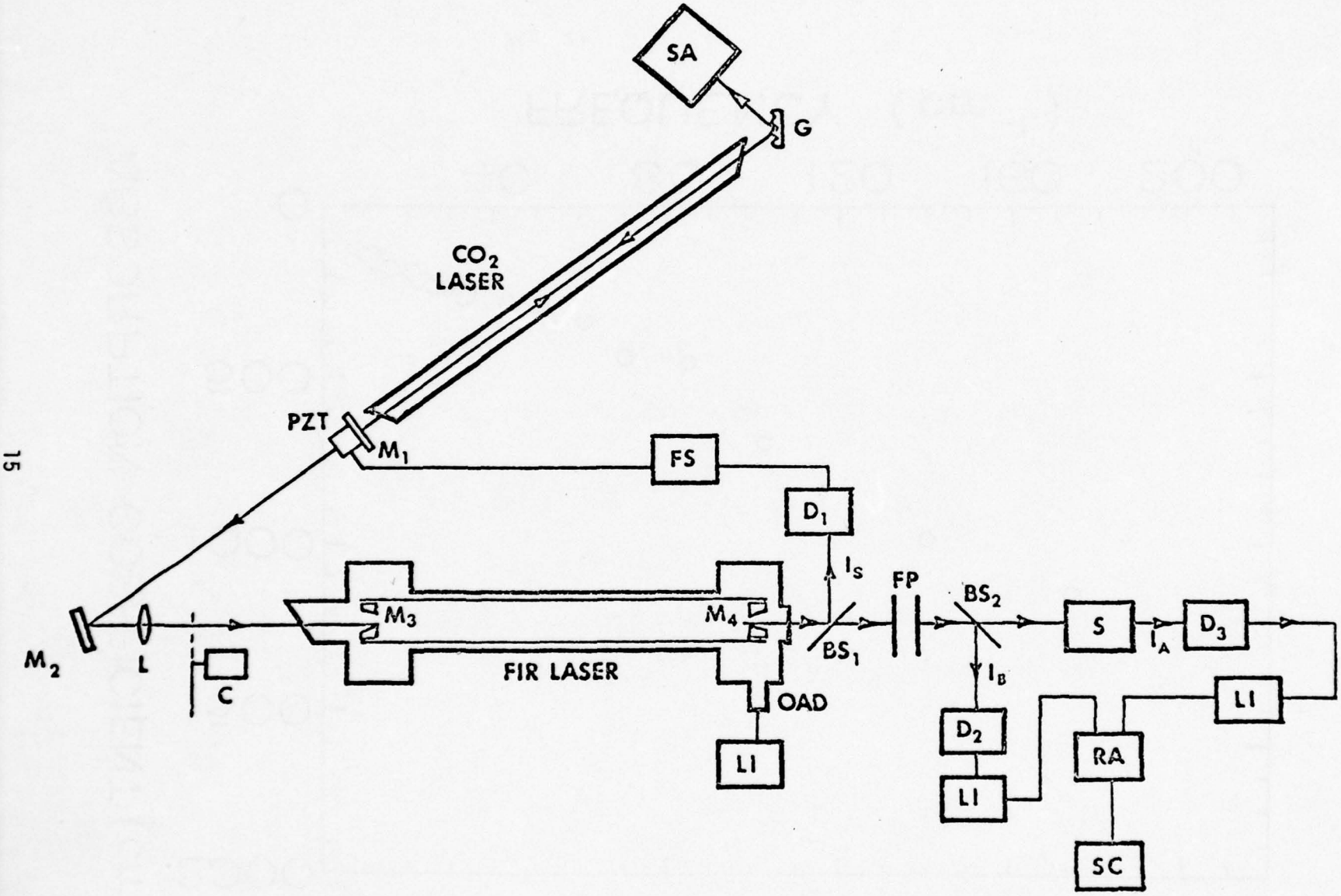
SA
G
CO_2 LASER
PZT
M_1
FS
D_1
I_S
FP
BS_2
S
I_A
D_3
M_2
L
C
M_3
M_4
BS_1
FIR LASER
OAD
LI
I_B
D_2
LI
RA
LI
SC

Fig. 1

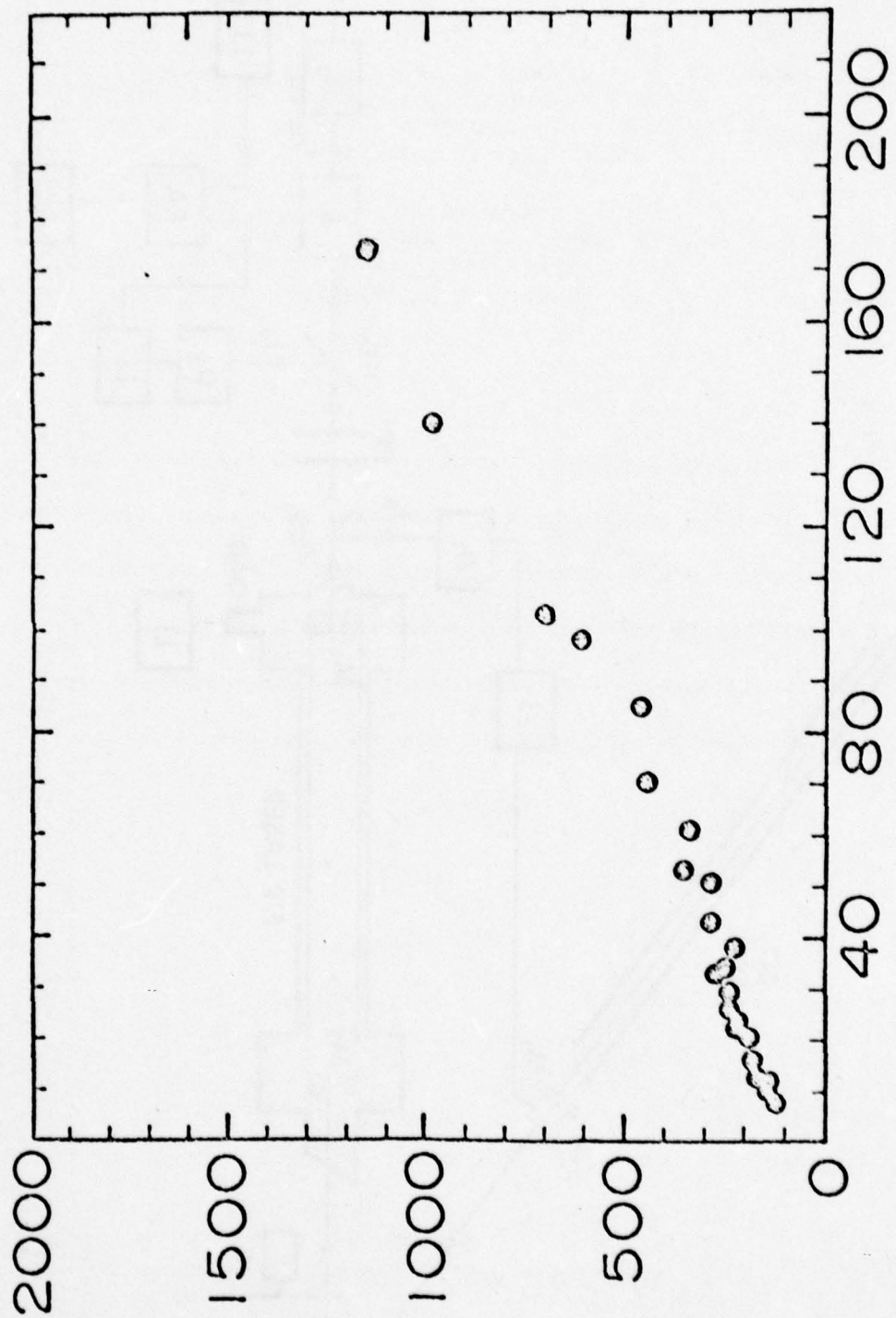
ABSORPTION COEFFICIENT (cm^{-1})
2000
1500
1000
500
0
40
80
120
160
200
FREQUENCY (cm^{-1})

Fig. 2

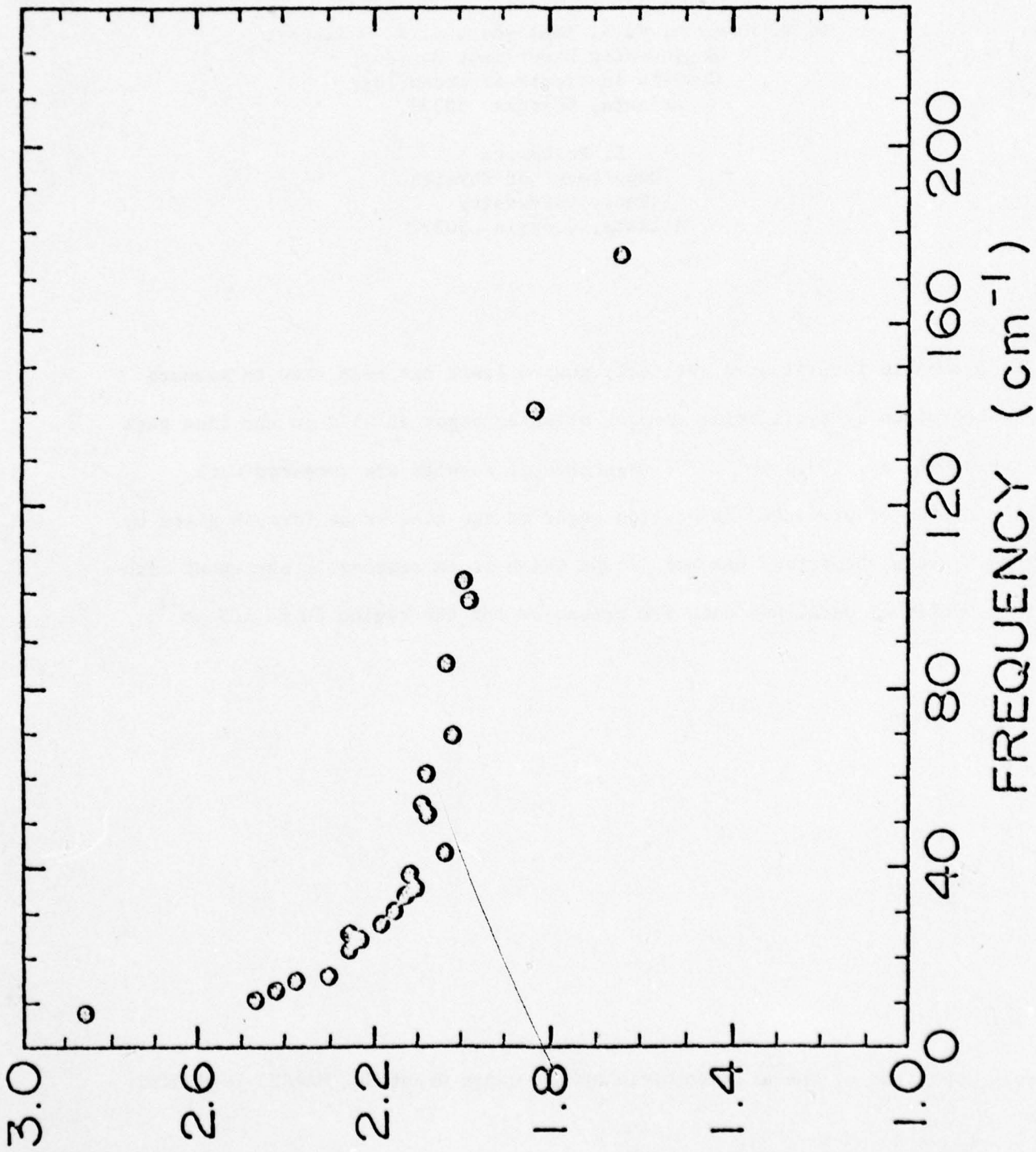
REFRACTIVE INDEX n
3.0
2.6
2.2
1.8
1.4
1.0
0
40
80
120
160
200
FREQUENCY (cm⁻¹)

Fig. 3

MEASUREMENTS OF FAR INFRARED WATER VAPOR ABSORPTION BETWEEN LINES WITH AN OPTICALLY PUMPED LASER*

O. A. Simpson, R. A. Bohlander, J. J. Gallagher
Engineering Experiment Station
Georgia Institute of Technology
Atlanta, Georgia 30332

S. Perkowitz
Department of Physics
Emory University
Atlanta, Georgia 30322

A tunable far-infrared optically pumped laser has been used to measure the absorption by equilibrium samples of water vapor at 25°C in the line gaps between 8.17 and 103.6 cm^{-1}. The experimental results are compared with calculations of predicted absorption based on the line shape formula given by Gross. Excess absorption has been found which is in reasonable agreement with other published data. New data are presented for the region 60 to 105 cm^{-1}.

*Work supported by the Army Research Office under Grant No. DAAG29-76-G-0280

I. INTRODUCTION

In the far infrared (FIR) or submillimeter spectral region water vapor is the dominant absorber in the atmosphere. Previous studies of water vapor, both in the laboratory and atmosphere have shown absorption between lines which is in excess of that predicted by existing line shape formulae.[1, 2, 3] This excess absorption has been attributed to errors in theoretical line shapes,[1] to water dimers,[2-7] and/or molecular aggregates or clusters.[8] Considering the recent growth of atmospheric applications in the FIR-submillimeter region, the lack of a firm understanding of how radiation and water molecules interact only underscores the need for more hard data from controlled experiments.

The present study is an initial effort to measure the absorption by equilibrium samples of water vapor of radiation from a tunable FIR optically pumped laser.[9] The use of a pumped FIR laser is a unique feature of our measurements. The high power of this device gives a signal-to-noise ratio which is superior to any other available broadband FIR source.

Data are presented for various water vapor pressures at 25°C for seven laser frequencies between 8.17 and 103.6 cm^{-1}. The frequencies chosen lie in the gaps between strong monomer lines as shown in Fig. 1 and were taken from the National Physical Laboratory table.[10] Only those frequencies well removed from line shoulders were chosen in order to minimize the error in predicted absorption due to uncertainty in the laser frequency. Although the family of discrete FIR laser lines does not provide continuous spectral coverage, there was no difficulty in finding lines which met this criteria.

Our measured absorptions are in excess of the theoretical values at each of the laser frequencies and at all pressures. The derived excess absorption agrees reasonably well with other published data obtained with Fourier spectrometers and HCN lasers and provides new information in the spectral region between 60 and 105 cm^{-1}.

II. THEORETICAL AND EXPERIMENTAL METHODS

The predicted absorption at each laser frequency was calculated using the line shape formula given by Gross[11, 12]:

$$\alpha(\nu) = \frac{nS}{\pi}\left[\frac{4\nu^2\delta}{(\nu^2 - \nu_o^2)^2 + 4\nu^2\delta^2}\right]$$

for the contribution of a line centered at wavenumber ν_o to the absorption coefficient α at wavenumber ν. Here δ is the half-width at half maximum, S is the line intensity, and n is the absorbing medium number density. There is very little difference in choosing the Gross formula over other commonly used line shape formulae (Van Vleck-Weisskopf, Lorentz, etc.). These are all based on instantaneous impact theory and give essentially idential results in the spectral region studied. The formula given by Van Vleck and Weisskopf[13] does predict less absorption below 15 cm^{-1}, but in this region excess absorption is large enough that the difference is not significant.

The water line frequencies, intensities, and initial state energies for

the 346 lines used were taken from the AFGL[14] table with self-broadening line width coefficients taken from calculations by Benedict and Kaplan[15]. The modification of line parameters for temperature and pressure was done as described by McClatchey with the exception of the temperature dependent exponent of the line widths, which were determined separately for each line from values of widths tabulated at two temperatures by Benedict and Kaplan.

The measurements were made with an optically pumped waveguide type FIR laser spectrometer, which is shown in block diagram form in Fig. 2. This apparatus has been extensively described elsewhere[16,17,18] and only relevant details will be given here. The laser provides a large selection of individual FIR lines with a typical power of milliwatts CW in each line. The frequencies have been determined with great accuracy by various workers, but as a precaution against possible error in the published laser frequencies, a Fabry-Perot interferometer was used to measure and confirm each of the seven wavelengths.

The water vapor was contained in a straight glass pipe absorption cell of length 3.44 m and diameter 10 cm. The ends of the cell had crystalline quartz windows offset 15° to the laser beam path. Initial measurements with the cell had resulted in much larger absorption than expected, which was determined to be due to interference effects. The offset of the windows was helpful in eliminating these interference effects, as were several co-axial absorbing bellows placed at several points along the cell. Distilled water

was evaporated and introduced into the cell through a perforated tube running the cell length. When sufficient vapor had entered the cell, the system was closed and allowed to reach equilibrium at room temperature, 25 $\pm$ 1°C. The static vapor pressure was measured with a Baratron MKS capacitance manometer, which had an accuracy of $\pm$2%.

To measure transmission the output from a Golay detector preceding the absorption cell was electronically divided into the output of another Golay detector following the cell. For each FIR laser frequency, several values of this ratio were determined for transmission through the cell evacuated and for various water vapor pressures. The resulting ratio of the two separately determined values then yielded the measured water vapor power transmission coefficient. This method has the important advantage of eliminating any fluctuations in the FIR power arising from laser instabilities. Measured values of the water vapor absorption at 43.649 cm^{-1} are shown in Fig. 3 as an example, together with the predicted absorption based on the Gross line shape.

The excess absorption coefficient was calculated according to the equation

$$\alpha_{excess} = -\ell n(T_M/T_G) \; / \; L$$

where L is the pathlength, T_M and T_G are the measured and theoretical transmission respectively. As shown in Fig. 4 for the frequency 43.649 cm^{-1}, a straight line showing excess absorption depending on density squared fits the data within experimental undertainty. Such a relationship, determined by an error weighted least squares fit was found for each of the other laser

frequencies. This result was expected, since in both speed of sound[19] and calorimetric data[20] the third and higher order virial terms have been reported to be negligible. The observed excess absorption, normalized to density squared, is shown in Fig. 5 for each of the laser frequencies.

III. DISCUSSION

In a study of molecular absorption one has to keep in mind the limitations of present line shape formulae that are based on the assumption of instantaneous collisions. Excluded from these, of course, are a wide range of possible molecular interactions. This particular weakness in theory introduces difficulties in interpreting new information; however, such formulae are widely used. Hence, calculations in the present study can be readily reproduced by other researchers.

Our measurements of the excess absorption in the FIR spectral region by water vapor are in general agreement with other reported work, but we have observed a somewhat larger excess absorption at 50 cm^{-1}. It should be noted that similar studies on water vapor with a HCN maser[2] also resulted in slightly greater excess absorption that that from broadband FIR source measurements. In addition, there is new evidence of an unexpected decrease in the excess absorption at higher frequencies. These results are preliminary and more laser lines will be used to increase resolution in this frequency region.

REFERENCES

1. D. E. Burch, J. Opt. Soc. Am. 58, 1383-1394 (1968).

2. W. J. Burrough, R. G. Jones, and H. A. Gebbie, J. Quant. Spectrosc. Radiat. Transfer 9, 809-824 (1969).

3. R. A. Bohlander, Ph.D. Thesis, Imperial College of Science and Technology, University of London (1979).

4. A. A. Viktorova, S. A. Zhevakin, Sov. Phys. - Dokl. 11, 1059-1062, 1065-1068. (1967).

5. A. A. Viktorova, S. A. Zhevakin, Sov. Phys. - Dokl. 15, 836-839, 852-855 (1971).

6. A. A. Viktorova, S. A. Zhevakin, IZV VUZ. Radiophys. 18, 211-221 (1975).

7. D. T. Llewellyn-Jones, R. J. Knight, and H. A. Gebbie, Nature 274, 876-878 (1978).

8. H. R. Carlon, "Introduction to Polymolecular Water Clusters and Their Infrared Activity," Draft Report, Defense Developm. Eng. Lab., U. S. Army, Edgewood Aresenal, Md., (1977).

9. T. Y. Chang and T. J. Bridges, Opt. Commun., 1, 423-425 (1970).

10. D. J. E. Knight, "Ordered List of Optically Pumped Laser Lines With Frequencies," National Physical Lab. Report No. Qu 45 (1979).

11. E. P. Gross, Phys. Rev. 97, 395-403 (1955).

12. R. J. Emery, Appl. Opt. 7, 1247 (1968).

13. J. H. Van Vleck and V. F. Weisskopf, Rev. Mod. Phys. 17, 227-236 (1945).

14. R. A. McClatchey, W. S. Benedict, S. A. Clough, D. E. Burch, R. F. Calfee, K. Fox, L. S. Rothmann, and J. S. Garing. AFCRL Atmospheric Absorption Line Parameters Compilation, Air Force Cambridge Research Laboratories Report AFCRL-TR-73-0096. (1973).

15. W. S. Benedict, L. D. Kaplan, J. Quant. Spectrosc. Radiat. Transfer 4, 453-469 (1964).

16. B. L. Bean and S. Perkowitz, Appl. Opt. 11, 2617 (1976).

17. B. L. Bean and S. Perkowitz, J.O.S.A. 67, 911-913 (1977).

18. O. A. Simpson, B. L. Bean, and S. Perkowitz, J.O.S.A., to be published.

19. R. A. Bohlander and H. A. Gebbie, Nature 253, 523-525 (1975).

20. J. A. Goff and S. Gratch, Trans. Am. Soc. Heat. Vent. Engrs. 52, 95-122 (1946).

FIGURE CAPTIONS

Figure 1a, b. Theoretical water vapor absorption based on the Gross line shape formula with laser frequencies in the gaps shown by arrows.

Figure 2. Block diagram of the FIR laser spectrometer: m, mirrors; G, grating; L, lens; SA, spectrum analyzer; PZT piezoelectric transducer; C, chopper; D, detectors; BS, beamsplitters; FP, Fabry-Perot interferometer; S, water vapor sample; LI, lock-in amplifier; RA, digital ratiometer; FS, frequency stabilizer, SC, stripchart recorder; OAD, opto-acoustic detector.

Figure 3. The measured water vapor absorption at 43.649 cm^{-1}. Theoretical absorption shown by X's for comparison.

Figure 4. Density dependence of excess absorption at 43.649 cm^{-1}. Straight lines fitted by weighted least squares.

Figure 5. Observed excess absorption coefficients divided by density squared for each laser frequency.

Fig. 1a

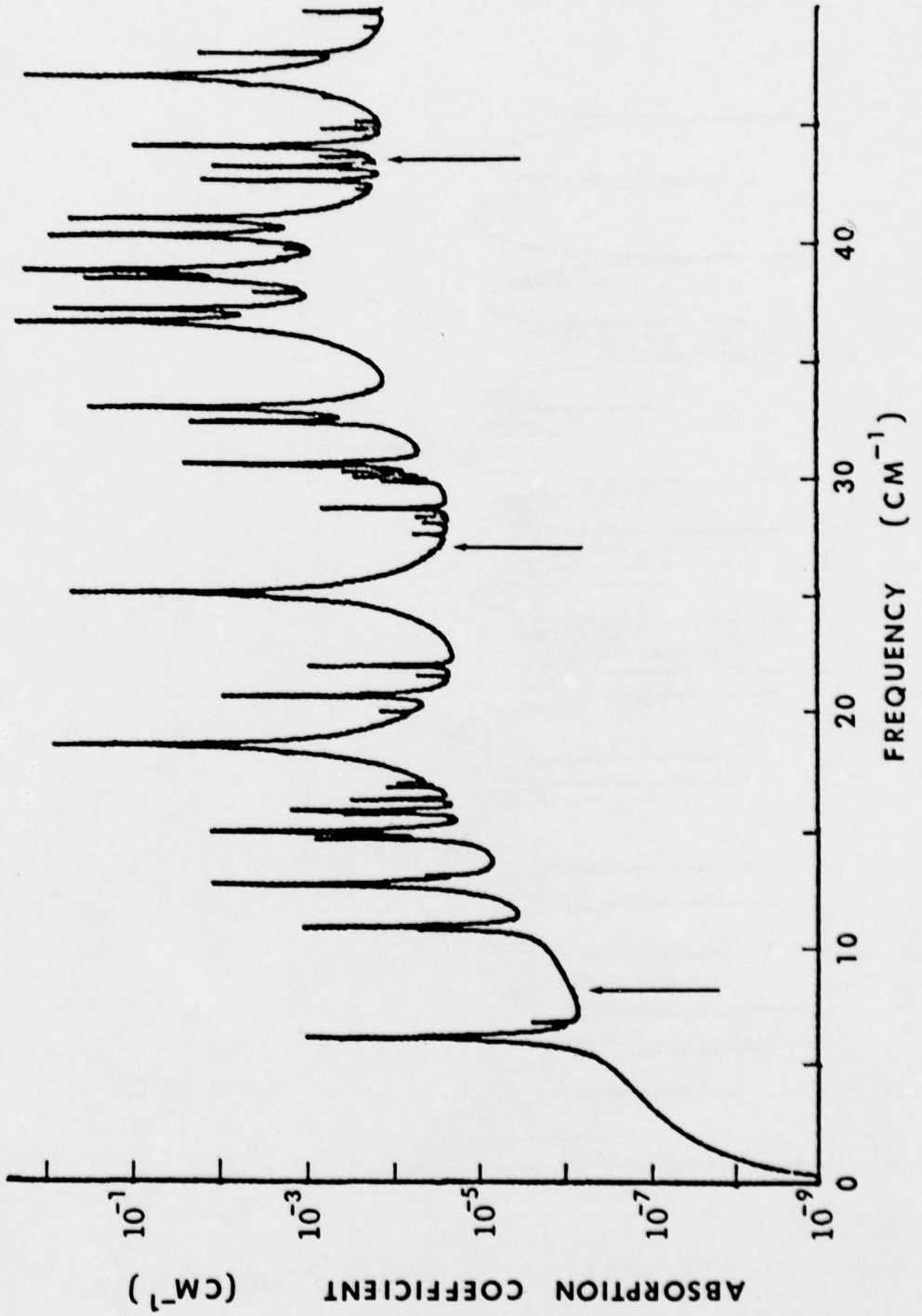
ABSORPTION COEFFICIENT (CM^{-1})
10^{-1}
10^{-3}
10^{-5}
10^{-7}
10^{-9}
0
10
20
30
40
FREQUENCY (CM^{-1})

Fig. 1b

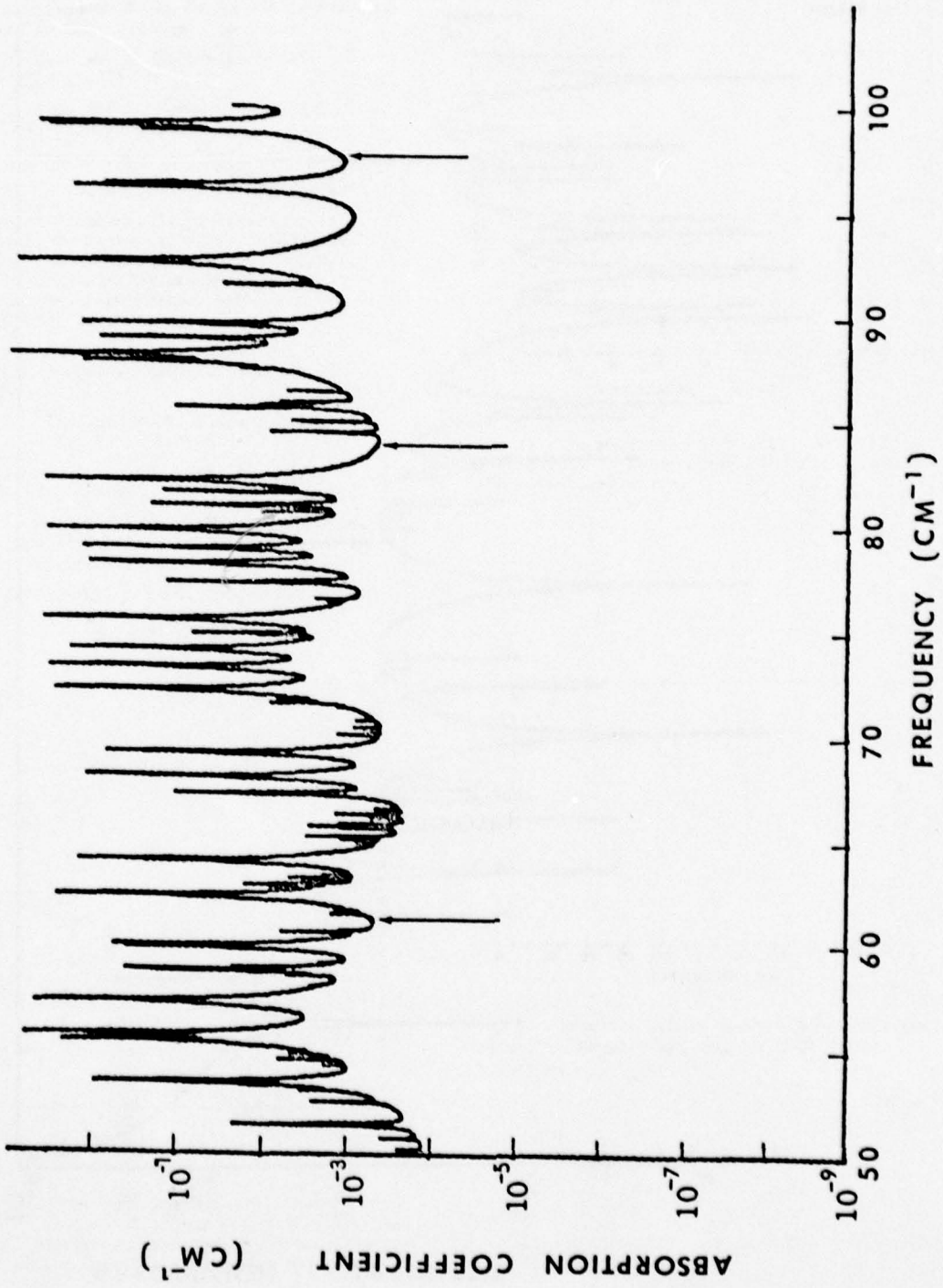
ABSORPTION COEFFICIENT (CM^{-1})
10^{-1}
10^{-3}
10^{-5}
10^{-7}
10^{-9}
50
60
70
80
90
100
FREQUENCY (CM^{-1})

Fig. 2

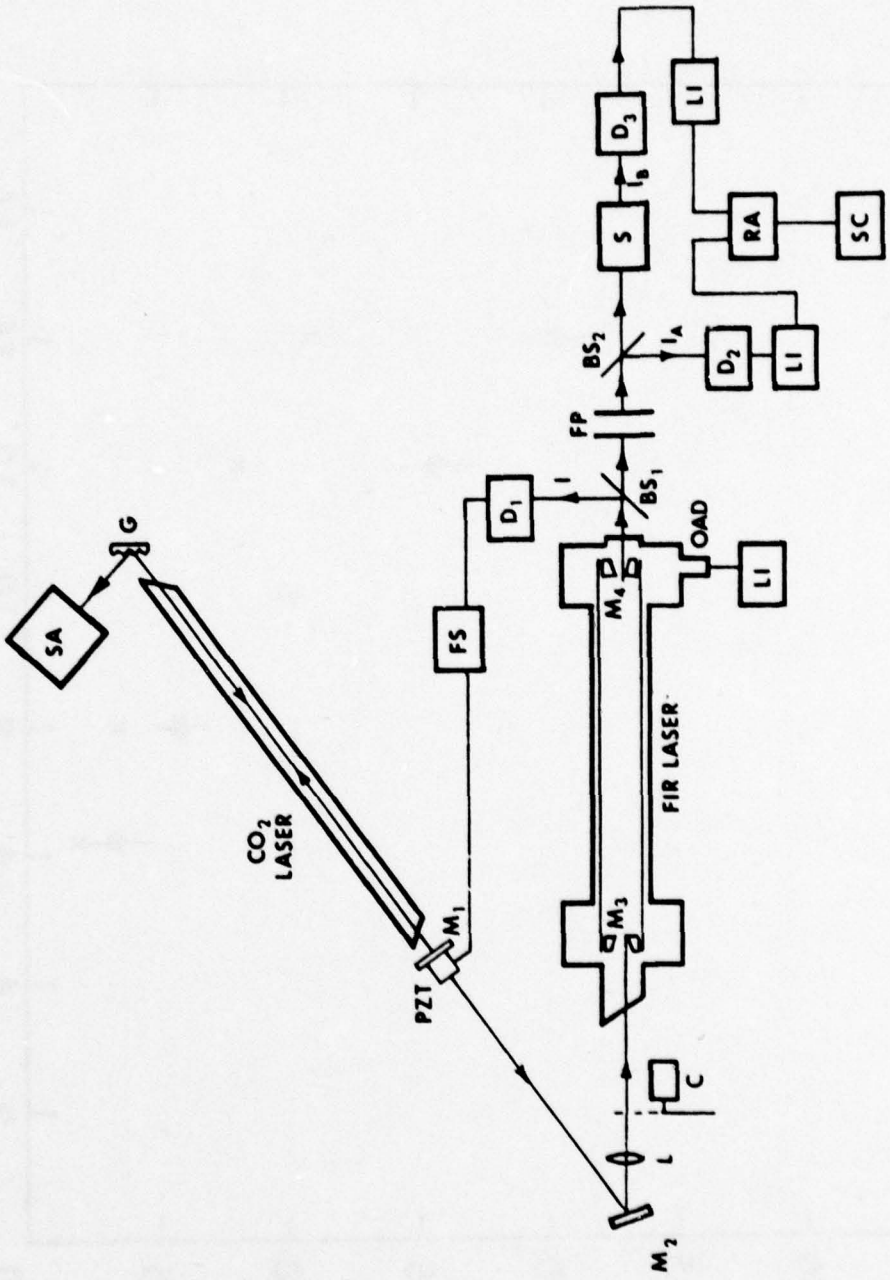
SA
G
CO_2 LASER
M_1
PZT
FS
D_1
I
BS_1
OAD
LI
M_4
M_3
FIR LASER
C
L
M_2
FP
BS_2
I_A
D_2
LI
S
I_B
D_3
LI
RA
SC

Fig. 3

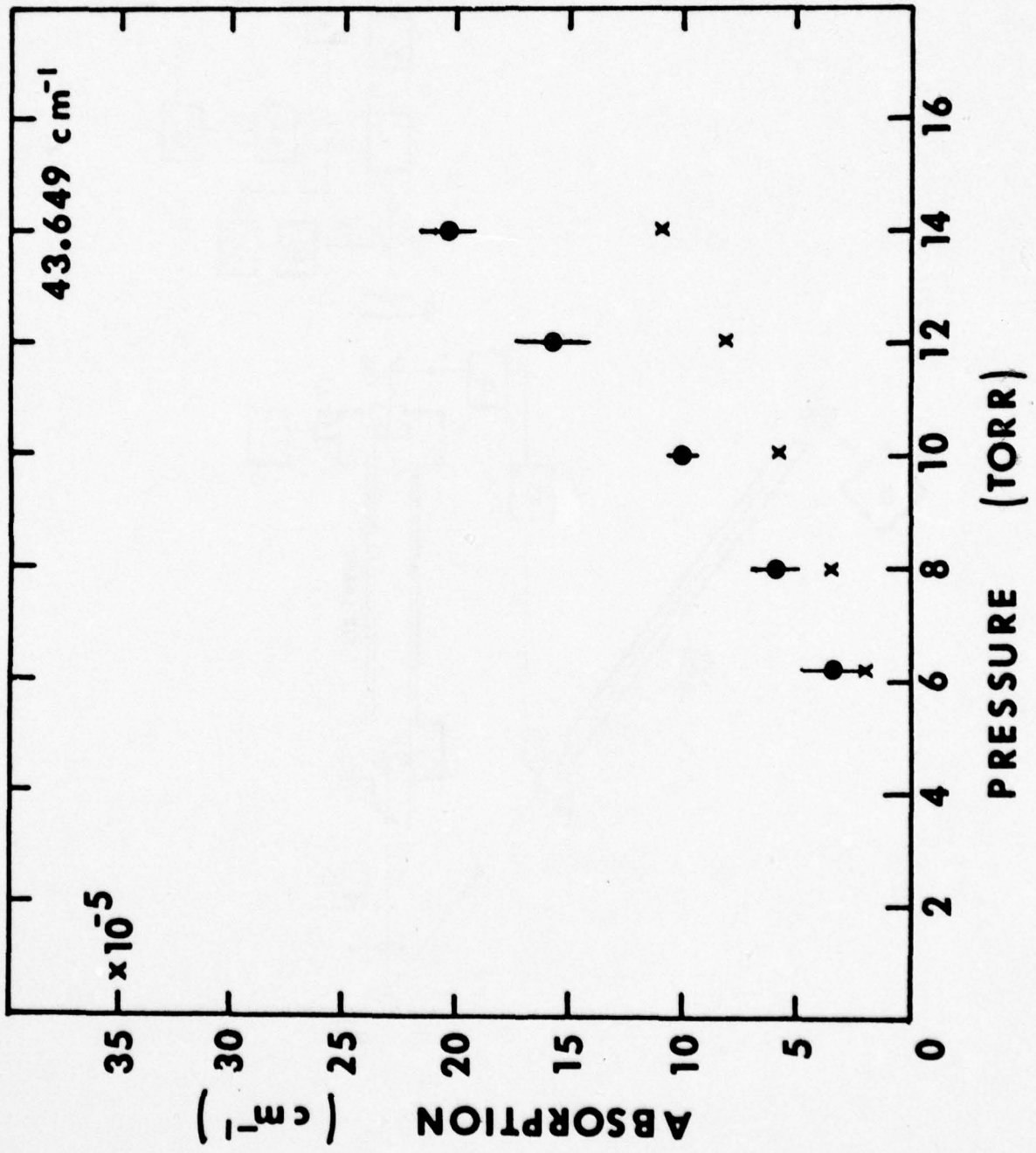
43.649 cm⁻¹
x10⁻⁵
35
30
25
20
15
10
5
0
ABSORPTION (cm⁻¹)
2
4
6
8
10
12
14
16
PRESSURE (TORR)

Fig. 4

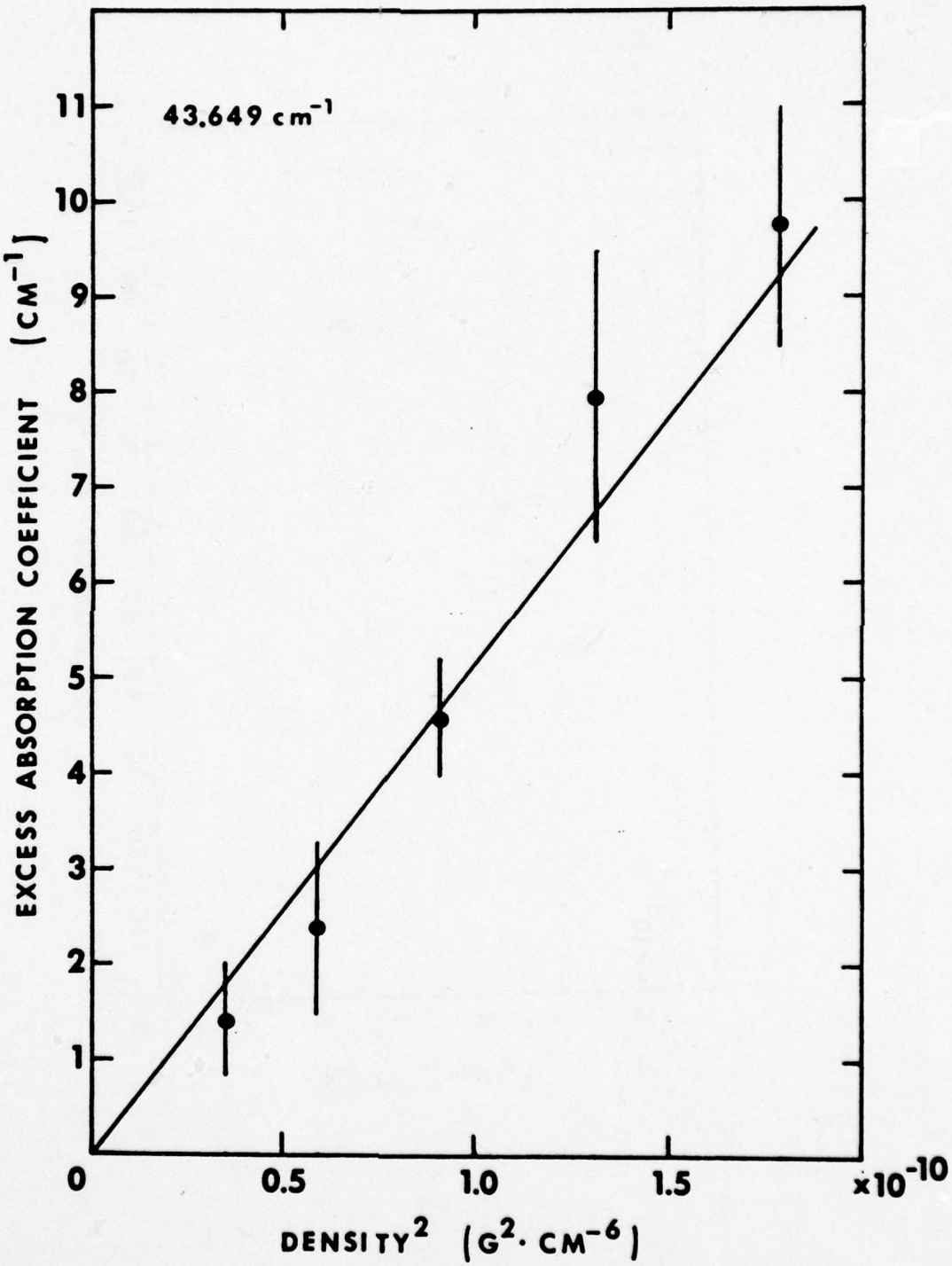
43.649 cm⁻¹
EXCESS ABSORPTION COEFFICIENT (CM⁻¹)
DENSITY² (G².CM⁻⁶)
0
0.5
1.0
1.5
x10⁻¹⁰
1
2
3
4
5
6
7
8
9
10
11

Fig. 5

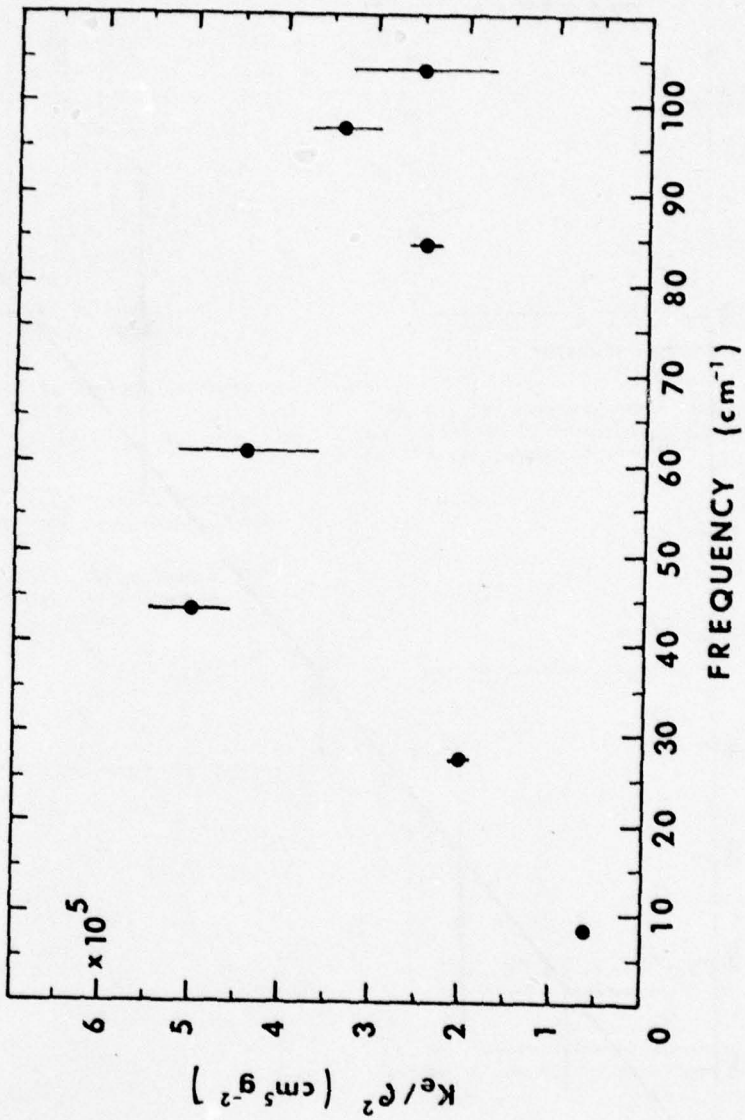
K_e/ρ^2 ($cm^3 g^{-2}$)
x 10^5
0
1
2
3
4
5
6
10
20
30
40
50
60
70
80
90
100
FREQUENCY (cm^{-1})

DIGEST OF THE FOURTH INTERNATIONAL CONFERENCE ON INFRARED AND MILLIMETER WAVES, MIAMI BEACH, FLORIDA, 10-15 DECEMBER, 1979

FAR-INFRARED LASER SPECTROSCOPY OF WATER VAPOR AND LIQUID WATER*

O. A. Simpson and S. Perkowitz
Physics Department
Emory University
Atlanta, Georgia 30322 U.S.A.

R. A. Bohlander and J. J. Gallagher
Engineering Experiment Station
Georgia Institute of Technology
Atlanta, Georgia 30332 U.S.A.

Introduction

We have used a far infrared (FIR) optically pumped laser to measure both the reflection and transmission of liquid water and the absorption by water vapor of radiation in the spectral region betwen 8.22 and 175.7 cm^{-1}. The pumped laser is a unique feature of our measurements. The high power of this device gives a signal-to-noise ratio which is superior to that available from broadband FIR sources.

The optical data for liquid water were used to determine the complex refractive index n-ik [1]. Data for measured absorption by water vapor were compared with calculations of predicted absorption based on the line shape formula given by Gross. Our measured absorptions are in excess of the theoretical values at each of the laser frequencies and at all pressures.

Experimental Methods and Results

The FIR laser was of the waveguide type and has been described elsewhere [1-3]. A ratioing process using two detectors was helpful in eliminating any fluctuations in the FIR power arising from laser instabilities.

Free surface measurements of the reflection coefficient $\Re$ were made on distilled water at 25 $\pm$ 1°C for near normal incidence with typical random errors under 1%. An adjustable pathlength cell was used to determine values of the liquid water transmission at increments of 5 μm to an accuracy of 1 μm over an average change in pathlength of 60 μm. The Lambert absorption coefficient α was determined at each laser frequency f by least squares fittings and used to calculate values of $k = \alpha/4\pi f$. Each k with the appropriate R was used to determine n from the normal incidence relation. The results for n are shown in Fig. 1.

Measurements of the absorption by water vapor were performed using a straight glass pipe absorption cell of length 3.44 m and diameter 10 cm. Distilled water was evaporated and introduced into the cell through a perforated tube running the cell length. To measure transmission the output from a Golay detector preceeding the absorption cell was electronically divided into the output of another Golay detector following the cell. The quotient of the two ratios for transmission through the evacuated cell and for various water vapor pressures yielded the measured water vapor power transmission coefficient.

The predicted absorption was calculated at each laser frequency using the line shape formula given by Gross [4,5]:

$$K(\nu) = \frac{ns}{\pi}\left[\frac{4\nu^2\delta}{(\nu^2-\nu_o^2)^2 + 4\nu^2\delta^2}\right]$$

for the contribution of a line centered at frequency ν_o to the absorption coefficient K at frequency ν. Here δ is the half-width at half maximum, s is the line intensity, and n is the absorbing medium number density. The water line frequencies, intensities, and initial state energies were taken from the AFGL [6] table with self-broadening line width coefficients taken from calculations by Benedict and Kaplan [7]. The modification of line parameters for temperature and pressure was done as described in the AFGL table with the exception of the temperature dependent exponent of the line widths, which were determined separately for each line from values of width tabulated at two temperatures by Benedict and Kaplan.

The excess absorption coefficient was calculated according to the equation

$$K_{excess} = -\ell n(T_M/T_G)/L$$

where L is the pathlength and T_M and T_G are the measured and theoretical transmission respectively. Measured values of the water vapor absorption at 43.649 cm^{-1} are shown in Fig. 2 as an example, together with the predicted absorption based on the Gross line shape. The observed excess absorption, normalized by the density squared is shown in Fig. 3 for each of the laser frequencies.

Conclusions

The FIR laser has made it possible to obtain highly precise data in liquid water. The liquid data cover a broader range than the results of Afsar [8], but agree well where they overlap. These two sets of laser data are the definitive FIR results on liquid water to date.

The derived excess absorptions of water vapor extend the frequency range of other published data obtained with Fourier spectrometers [9,10] and HCN lasers [10,11] and provide new information in the spectral region between 60 and 105 cm^{-1}.

*This work was partially supported by the Army Research Office.

References

[1] O. A. Simpson, B. L. Bean, and S. Perkowitz, J. Opt. Soc. Am., in press.

[2] B. L. Bean and S. Perkowitz, Appl. Opt. 11, 2617 (1976).

[3] B. L. Bean and S. Perkowitz, J. Opt. Soc. Am. 67, 911-913 (1977).

[4] E. P. Gross, Phys. Rev. 97, 395-403 (1955).

[5] R. J. Emery, Appl. Opt. 7, 1247 (1968).

[6] R. A. McClatchey, W. S. Benedict, S. A. Clough, D. E. Burch, R. F. Calfee, K. Fox, L. S. Rothmann, and J. S. Garing, AFCRL Atmospheric Absorption Line Parameters Compilation, AFCRL Report AFCRL-TR-73-0096(1963).

[7] W. S. Benedict and L. O. Kaplan, J. Quant. Spectros. Radiat. Transfer 4, 453-469 (1964).

[8] M. N. Afsar and J. B. Hasted, Infrared Physics 18, 835 (1978).

[9] D. E. Burch, J. Opt. Soc. Am. 58, 1383-1394 (1968).

[10] R. A. Bohlander, Ph.D. Thesis, Imperial College of Science and Technology, University of London (1979).

[11] W. J. Burroughs, R. G. Jones, and H. A. Gebbie, J. Quant. Spectrosc. Radiat. Transfer 9, 809-824 (1969).

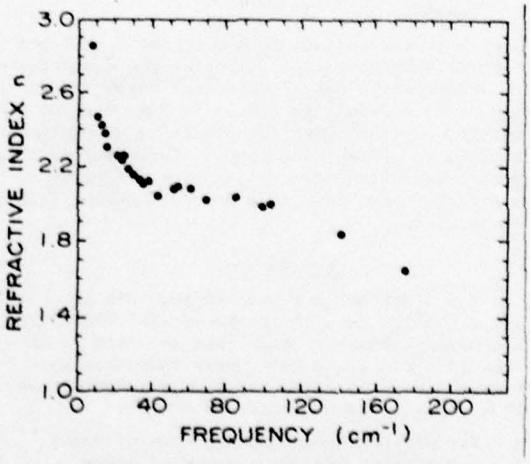

Fig. 1. Laser results for the real part of the index of refraction of liquid water at 25°C. The symbols for the laser experimental points are slightly larger than the typical random errors.

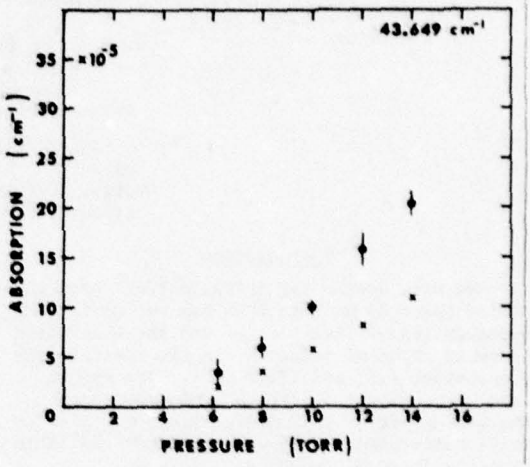

Fig. 2. The measured water vapor absorption at 43.649 cm^{-1}. Theoretical absorption shown by X's for comparison.

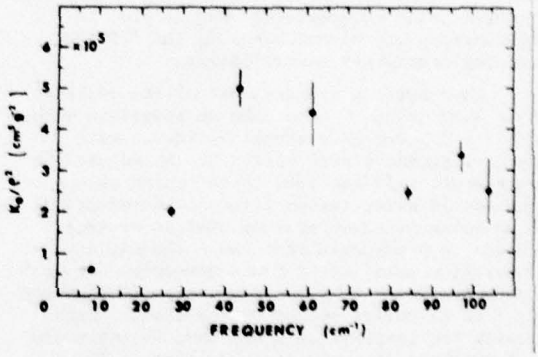

Fig. 3. Observed excess absorption coefficients divided by density squared for each laser frequency.

Excess Absorption by Water Vapor and Comparison with Theoretical Dimer Absorption

R. A. Bohlander
Appleton Laboratory, Slough, England
Present address: Georgia Institute of Technology
Engineering Experiment Station
Atlanta, Georgia 30332

R. J. Emery and D. T. Llewellyn-Jones
Appleton Laboratory, Slough, England

G. G. Gimmestad
University of Colorado, Boulder, Colorado
Present address: Michigan Technological University
Keweenaw Research Center, Houghton, Michigan 49931

H. A. Gebbie
Imperial College of Science and Technology
University of London, London, England

O. A. Simpson and J. J. Gallagher
Georgia Institute of Technology
Engineering Experiment Station
Atlanta, Georgia 30332

S. Perkowitz
Department of Physics
Emory University
Atlanta, Georgia 30332

ABSTRACT

Absorption by water vapor has been measured in wavenumber ranges from 8 to 105 cm^{-1} and 300 to 600 cm^{-1}. The excess over prediction with the Gross line shape has been compared with theoretical dimer absorption. The temperature dependence and over-all magnitude of excess absorption are in reasonable agreement with prediction for dimers, but the shape is different. The limitations of the present theory of dimer absorption are discussed.

1. Introduction

It is well-known that established line shape formulas based on an impact approximation are unable to predict molecular absorption in the wings of absorption lines. In the case of water, observed absorption has been found to exceed prediction in the gaps between lines from the microwave to the infrared regions of the spectrum. The desire for a better theoretical model has been spurred by interest in the propagation of radiation through water vapor in the atmosphere.

To get an improved theory of the shape of water vapor absorption lines, more detailed information about molecular interactions during collisions will be needed than is available at the present time. Since two water molecules can form a weak hydrogen bond, dimers have also been suggested (Viktorova and Zhevakin 1967, 1971, 1975) as another possible source of excess absorption. This paper reports studies of excess absorption in the laboratory in the wavenumber ranges 8 to 105 cm^{-1} and 300 to 600 cm^{-1}, and comparisons are made with a calculated theoretical spectrum of water dimers. This is in the nature of a progress report and is not a definitive test of whether dimers are important since there are significant limitations in our understanding of dimer structure at normal temperatures. Many of the details of this study have been given in the thesis of Bohlander (1979) and further publications will follow.

2. Excess Absorption--Definition

One cannot measure excess absorption *per se*: it is the difference between observed absorption and prediction based on a line shape formula. Thus it is important to define carefully how the prediction is made. We have used the parameters for the frequency, intensity, and widths of lines given by McClatchey et al. (1973), Benedict and Kaplan (1963), Flaud, Camy-Peyret and co-workers (1976, 1977), and Toth and Margolis (1975). Commonly used line shape formulas are the Gross or kinetic line shape formula (Gross 1955), the Van Vleck-Weisskopf formula, and the modified Lorentz

formula (Van Vleck and Weisskopf 1945), and from these there is little to choose theoretically. They all invoke the key assumption that collisions are instantaneous. We have chosen the Gross formula. Numerical results with the formulas mentioned are negligibly different in the wavenumber range studied except with the Van Vleck-Weisskopf formula below 15 cm^{-1}. It predicts somewhat less absorption, but the conclusions of this paper would not be changed if this formula had been used.

Preliminary predictions of the absorption spectrum were made including all the pure rotation band lines in the calculation. We then made shortened tables of lines from which predictions in 50 cm^{-1} intervals differed negligibly* from a full calculation. In this way typically 400 and no more than 700 lines were needed at any given frequency for subsequent calculations, compared with 2600 pure rotation lines below 700 cm^{-1} in the complete tabulation we used.

Some workers have used much more abbreviated lists of lines in their calculation of the pure rotation line absorption (see eg. Burch 1968; Burch et al. 1974; Frenkel and Wood 1964; Gaut and Reifenstein 1971): they have selected only lines near the frequency of interest. Excess absorption in this case varies slowly with frequency and can be incorporated in an easy-to-use empirical formula to predict absorption. However, in physical terms, these selections of lines are rather arbitrary and cause confusion when values of excess absorption are compared, since allowance must be made for the various omissions of absorption lines. Moreover, observations have shown that some of the empirical formulations have oversimplified the dependence of absorption on the water vapor density and temperature. We have determined these dependences from observations and will consider them in relation to the dimer model.

*The tolerance was 0.2 dB/km for a water vapor density of 26 g m^{-3}.

3. Theoretical Dimer Absorption

We have made theoretical calculations of the absorption spectrum of dimers from existing information about their structure. A number of theoretical chemists have made molecular orbital calculations in order to find the hydrogen bond energy and the most stable structure, shown in Figure 1. Dill et al. (1975) give a useful review, and more recent work is described by Matsuoka et al. (1976). These predictions were found to be consistent with high resolution measurements (Dyke et al., 1977) of microwave transitions between rotation levels in the ground vibrational state of dimers in molecular beams. Therefore, the ground vibrational state appears to be well-understood in terms of the predicted lowest energy structure.

Since the hydrogen bond is weak, the water dimer has low-lying vibration levels, and only four percent of the population is estimated to be in the ground vibrational state at normal temperatures. Thus it is an important question whether dimers retain approximately the lowest energy configuration at these temperatures. Using an empirical model* of the potential energy between two water molecules, Owicki, Shipman and Scheraga (1975) have concluded that barriers to internal rotation are low. In this situation the orientations of the two water molecules in a dimer would not be well-confined to configurations near the lowest energy one. We felt it was probably premature, and was in any case a difficult problem, to try to calculate a theoretical dimer spectrum that would take account of internal rotation. Rather we have calculated a theoretical spectrum for the more tractable case in which the dimer is assumed to undergo rigid rotation and small-amplitude harmonic vibration. Comparison with the spectrum of excess absorption in water vapor has been used as a test of this theory and as an indication whether there may be the need to consider internal rotation.

The dimer's expected pure rotation band in the rigid rotor approximation comes at a low frequency because the dipole moment (2.6 D) measured by Dyke et al. (1977) was found to be nearly parallel to the line between the heavy oxygen atoms. The peak of the predicted band is at 16 cm^{-1} (480 GHz) as shown in Figure 2. One might expect the spectrum to be almost that of a symmetric top with a rotation inertial constant of 0.2 cm^{-1} and with only small perturbations due to the light hydrogen atoms. Early calculations of the dimer spectrum were made on that basis (Viktorova and Zhevakin 1967, 1971, 1975;

*Electrons and nuclei were placed in fixed positions to reproduce the dipole moment of water and the structure of ice.

Braun and Leidecker 1974). However, molecular beam studies (Dyke et al. 1977) have shown a much more complicated spectrum below 1.6 cm^{-1}(48 GHz). This is attributed to inversion tunnelling, but few assignments of the observed lines have been made. Therefore, we have not attempted to calculate rotational structure in detail and have used smoothed band contours.

The remainder of the predicted absorption is assigned to six intermolecular vibration modes involving the hydrogen bond. We have calculated the normal intermolecular vibrational frequencies for the dimer from a recent molecular orbital study of intermolecular potential energy (Matsuoka et al., 1976).* ** Most of the modes involve partial rotation of the monomers within the dimer, and, since this causes large dipole moment oscillations, the predicted absorption intensity is large. Intensities were calculated with the assumption that the charge distribution remains fixed on the monomer units during vibrations.**

In addition, we need to know the number density of dimers to be able to calculate their absorption in dB/km. Although dimers have been observed in molecular beams, we know nothing from this about equilibrium concentrations. These we have estimated in the usual way (see e.g. Bolander et al. 1969) from experimental values of the second virial coefficient (Goff and Gratch, 1946). Typical calculated dimer concentrations are of the order of a part in 1000 of the monomer concentration. Uncertainties in the theory on which these calculations are based will be discussed later. Dimer concentrations are proportional to the square of the water vapor density, and their dependence on temperature is determined by the hydrogen bond energy. The best theoretical values of the latter are around .15 to .16 eV; the value estimated from the temperature dependence of the second virial coefficient is 0.12 eV (Bohlander, 1979).

*There is fairly good agreement between the vibration force constants from this study and those from other recent molecular orbital studies (Curtiss and Pople 1975; Kistenmacher et al. 1974).

**Values of the frequencies and intensities are also in reasonable agreement with those found by Owicki et al. (1975) using an empirical potential energy model.

4. Observations in the Laboratory

The spectral ranges that are most accessible to experimental study are in the wings of the monomer pure rotation band and include the predicted dimer pure rotation band and the predicted bands for hydrogen bond bending. We have studied water vapor without a foreign broadening gas since this would give the widest possible spectral ranges in which to search for dimer absorption. Uncertainties in the theory of collision broadening by a foreign gas are also avoided.

We began the study using Fourier transform spectroscopy and wide-band radiation taken from Mercury lamp or glow bar sources. Helium-cooled bolometers and Golay cell detectors were used. For the spectral ranges 12 to 50 cm^{-1} and 300 to 600 cm^{-1}, White-type absorption cells provided path lengths between 20 and 200 meters. A selection of observed spectra is given in Figure 3. They represent one minus the ratio of spectra obtained with a sample and with a vacuum in the absorption cell. The dashed curves show expected monomer absorption. One can see that in the gaps between lines in these wavenumber ranges, excess absorption is a considerable fraction of the total. Whether the excess absorption was due to collisions between two molecules or due to dimers, it was expected that it would be proportional to the density squared, and this was found to be true within experimental certainty.

Due to the presence of numerous strong monomer lines, one can get only a fragmentary picture of the excess absorption's spectral shape, as shown for the near millimeter region in Figure 4. Some results of Burch (1968) and Burroughs et al. (1969) are shown to be in good agreement. Measurements were also made by one of us (DLJ) with an HCN maser and are shown in the figure at 29.7 cm^{-1}. Some of these measurements were made with a large untuned cavity which Llewellyn-Jones will discuss elsewhere in these proceedings. He will also present further data in the range 2 to 15 cm^{-1} obtained with this facility.

At Georgia Tech and Emory University, two of us (O. A. S. and S. P.) have embarked on new measurements with an optically pumped laser described elsewhere (Bean and Perkowitz 1976, 1977). Preliminary results are shown

with solid circles. There is the potential for more precise measurements because of the power and stability of the laser, and, as shown, this is being used to extend the frequency range covered. The absorption cell is a straight pipe 3.4 m long designed to be used with a single pass through it. However, there has been difficulty in eliminating multiple passes arising from stray reflections. This has been largely corrected with baffles, but there is possibly a residual effect which may explain why these data show somewhat larger excess absorption at lower wavenumbers than previous data.

The integral of the observed excess absorption shown in Figure 4 is about the same as that predicted by the dimer model, but the shape of the spectrum is different. This is also true for the higher wavenumber range studied (Figure 5). Here observed excess absorption is represented by a smooth curve that fits our data and that of Burch et al. (1974) within the experimental uncertainty. As previously noted by Roberts et al. (1976), this seems to have the form of an exponential decrease with frequency in the range 300 to 600 cm^{-1}. Further discussion of the shape of excess absorption will be given, following consideration of the observed temperature dependence.

Typical results in the low and high frequency regions are given in Figure 6. The excess absorption data are plotted in this way to find the value of the energy E that characterizes the temperature dependence; this in turn can be compared with the estimated dimer energy of formation. The dotted lines show the temperature dependence of the predicted monomer component of the absorption. This is governed mainly by the Boltzmann distribution of the energy levels from which nearby absorption transitions arise; the slope therefore switches sign from one side of the monomer pure rotation band to the other. The temperature dependence of the excess absorption is more nearly uniform. Values of E given in Figure 7 are near the dimer energy of formation estimated from the temperature dependence of the second virial coefficient (Bolander et al. 1969; Bohlander, 1979).

5. Discussion

There are in general terms two possible ways of interpreting the discrepancy between the shape of observed excess absorption and that of predicted dimer absorption:

(1) Dimers at normal temperatures may have significantly different mean structures than they have at low temperatures, or

(2) The contributions by dimers to the excess absorption may be less important than possible contributions by unbound molecular pairs, i.e., there may be additional collision broadening of monomer lines.

Although hydrogen-bonded complexes are floppy species, it was not entirely unreasonable to try the assumption that water dimers vibrate harmonically with small amplitudes. Thomas (1975) has found vibration bands of the complex H_2O—HF which were easily recognizable despite some anharmonicity. Of course, H_2O—HF has a much higher binding energy than the water dimer (an energy of formation of ~ 0.3 eV instead of 0.12 eV), and this may mean that barriers to internal rotation are also higher. If water dimers have low barriers to internal rotation, this type of internal motion could be more important than vibration, and the mean dimer structure could be significantly different than it is at low temperatures. In studies of the more weakly bound van der Waals' complexes, examples have been found of vibrating species, of internally rotating species, and of intermediate cases (Ewing 1976). According to the theoretical study made of barriers of internal rotation by Owicki et al. (1975), mentioned earlier, there are five barriers and three of them have heights less than 100 cm^{-1}. Since 1/2 kT is of this order, it is likely that internal rotation is important at normal temperatures. Further exploration of the barriers with molecular orbital methods would be of interest.

The other principal assumption we have made in calculating theoretical dimer absorption is that the second virial coefficient of water vapor is entirely due to the presence of dimers, and on this assumption we have estimated the concentration of dimers. It is interesting that the excess absorption derived from observations is similar in magnitude to the predicted dimer absorption. However, the principle of spectroscopic stability can be applied here according to rules given by Gordon (1963), and one finds that any pair of water molecules, whether they are bound or unbound, will have about the same integrated absorption cross-section at frequencies in the far infrared (below the frequencies of the vibration bands of the monomer). It follows that we are not able to say from our measurements whether the second virial coefficient and the excess absorption are due to bound or unbound species.

Present theories discount the importance of unbound pairs at normal temperatures, but there are some simplifications made. For molecules with a spherically symmetric form of potential energy, Stogryn and Hirschfelder (1959) have shown that dimers are responsible for nearly all of the second virial coefficient when the dimer binding energy exceeds kT. In the case of water, the energy of dimer formation is more than 4kT, but it is not known whether the generalization of Stogryn and Hirschfelder can be extended to the case of molecules of low symmetry, such as water. Calculations of dimer concentrations may also be done from a knowledge of the intermolecular potential energy (Viktorova and Zhevakin 1971; Braun and Leidecker 1974; Lane 1975; Lie and Clementi 1976: Bohlander 1979). While reasonable agreement with experimental values of the second virial coefficient have been obtained in recent calculations, much uncertainty remains about the reliability of the approximations made. Therefore, the possibility of a significant contribution by unbound pairs to excess absorption cannot be ruled out.

6. Conclusions

(1) We have found that excess absorption by water vapor is similar in magnitude to predicted dimer absorption and has a similar temperature dependence.

(2) There are large discrepancies between the shape of excess absorption and that predicted for dimers.

(3) Further theoretical work is needed on internal rotation in dimers and on the theoretical concentrations of dimers at normal temperatures.

7. Acknowledgements

This work was supported in part by the Appleton Laboratory (U.K. Science Research Council), by the U.S. Army Research Office, and by NATO.

8. References

Bean, B. L. and Perkowitz, S. 1976, Appl. Opt. 15, 2617-2618.

Bean, B. L. and Perkowitz, S. 1977, J. O. S. A. 67, 911-913.

Benedict, W. S. and Kaplan, L. D. 1964 J. Quant. Spectrosc. Radiat. Transfer 4, 453-469.

Bohlander, R. A. 1979 Ph.D. Thesis, Imperial College of Science and Technology, University of London.

Bolander, R. W., Kassner, J. L. and Zung, J. T. 1969 J. Chem. Phys. 50, 4402-4407.

Braun, W. C. and Leidecker, H. 1974 J. Chem. Phys. 61, 3104-3113.

Burch, D. E. 1968 J. Opt. Soc. Am. 58, 1383-1394.

Burch, D. E., Gryvnak, D. A. and Gates, F. J. 1974 Continuum absorption by H_2O between 330 and 825 cm^{-1}, Air Force Cambridge Research Laboratories Report, AFCRL-TR-74-0377.

Burroughs, W. H., Jones, R. G. and Gebbie, H. A. 1969 J. Quant. Spectrosc. Radiat. Transfer 9, 809-824.

Camy-Peyret, C., Flaud, J. M., Maillard, J. P. and Guelachvili, G. 1977 Mol. Physics 33, 1641-1650.

Curtiss, L. A. and Pople, J. A. 1975, J. Mol. Spectrosc. 55, 1-14.

Dill, J. D., Allen, L. C., Topp, W. C. and Pople, J. A. 1975 J. Am. Chem. Soc. 97, 7220.

Dyke, T. R. 1977 J. Chem Phys. 66, 492-497.

Dyke, T. R., Mack, K. M. and Muenter, J. S. 1977 J. Chem. Phys. 66, 498-510.

Ewing, G. E. 1976, Can. J. Phys. 54, 487-504.

Flaud, J.-M., Camy-Peyret, C. and Maillard, J. P. 1976 Mol. Physics 32, 499-521.

Frenkel, L. and Woods, D., 1966, Proc. IEEE 54, 498-505.

Gaut, N. E. and Reifenstein, E. C. 1971, Environmental Research and Technology, Report No. 13, Concord, Mass.

Goff, J. A. and Gratch. S. 1946 Trans. Am. Soc. Heat. Vent. Engrs. 52, 95-122.

Gordon, R. G. 1963 J. Chem. Phys. 38, 1724-1729.

Gross, E. P. 1955, Phys. Rev. 97, 395-403.

Gryvnak, D. A., Burch, D. E., Alt, R. L. and Zgonc, D. K. 1976 Infrared Absorption by CH_4, H_2O, and CO_2, Air Force Geophysics Laboratory Report AFGL-TR-76-0246.

Kistenmacher, H., Lie, G. C., Popkie, H. and Clementi, E. 1974, J. Chem Phys. 61, 546-561.

Lane, J. G. 1965 J. Chem. Phys. 62, 1605-1606.

Lie, G. C. and Clementi, E. 1976 J. Chem. Phys. 64, 5308-5309.

McClatchey, R. A., Benedict, W. S., Clough, S. A., Burch, D. E., Calfee, R. F. Fox, K., Rothmann, L. S. and Garing, J. S. 1963 AFCRL Atmospheric Absorption Line Parameters Compilation, Air Force Cambridge Research Laboratories Report AFCRL-TR-73-0096.

Matsuoka, O., Clementi, E. and Yoshimine, M. 1976 J. Chem. Phys. 64, 1351-1361.

Roberts, R. E., Selby, J. E. A. and Biberman, L. M. 1976 Appl. Opt. 15, 2085-2090.

Stogryn, D. E. and Hirschfelder, J. O. 1959 J. Chem. Phys. 31, 1531-1545. Errata. (1960) J. Chem. Phys. 33, 942-943.

Thomas, R. K. 1975 Proc. R. Soc. Lond. A 344, 579-592.

Toth, R. A. and Margolis, J. S. 1975 J. Mol. Spectrosc. 57, 236-245.

Van Vleck, J. H. and Weisskopf, V. F. 1945 Rev. Mod. Phys. 17, 227-236.

Viktorova, A. A. and Zhevakin, S. A. 1967 Sov. Phys. - Dokl. 11, 1059-1062, 1065-1068.

Viktorova, A. A. and Zhevakin, S. A. 1971 Sov. Phys. - Dokl. 15, 836-839, 852-855.

Viktorova, A. A. and Zhevakin, S. A. 1975 Izv. VUZ. Radiophys. 18, 211-221.

KNOWN LOWEST ENERGY DIMER STRUCTURE

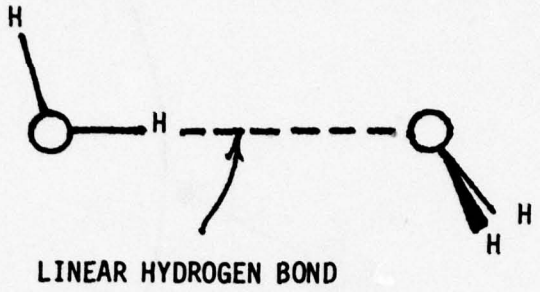

LINEAR HYDROGEN BOND

DIMER DIPOLE 2.6 D

=

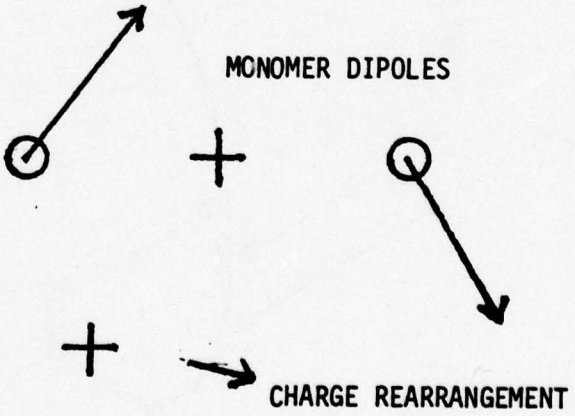

Figure 1

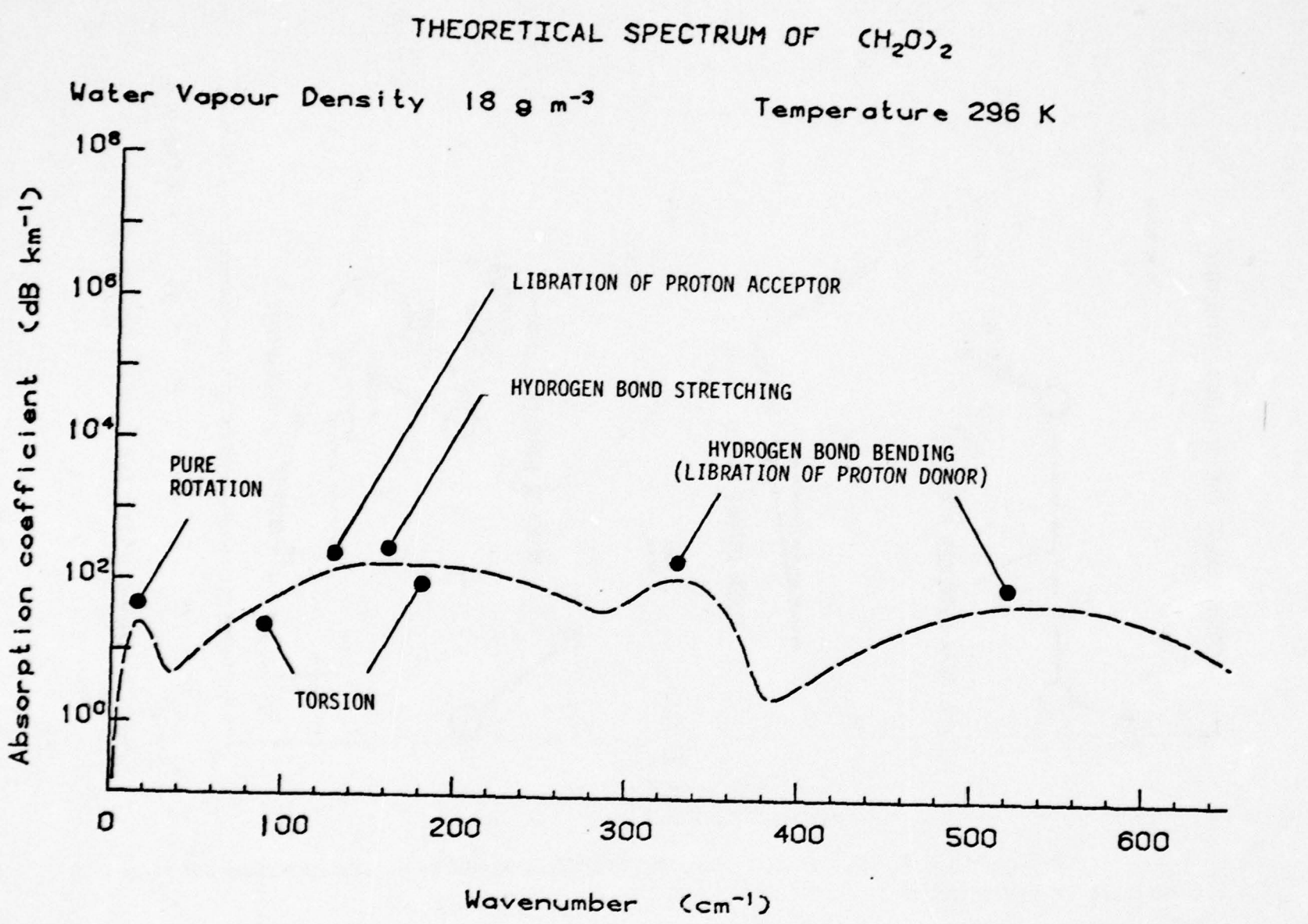
THEORETICAL SPECTRUM OF $(H_2O)_2$
Water Vapour Density 18 g m^{-3}
Temperature 296 K
Absorption coefficient (dB km^{-1})
10^8
10^6
10^4
10^2
10^0
LIBRATION OF PROTON ACCEPTOR
HYDROGEN BOND STRETCHING
HYDROGEN BOND BENDING
(LIBRATION OF PROTON DONOR)
PURE
ROTATION
TORSION
0
100
200
300
400
500
600
Wavenumber (cm^{-1})

Figure 2

ABSORPTION SPECTRUM OF WATER VAPOR

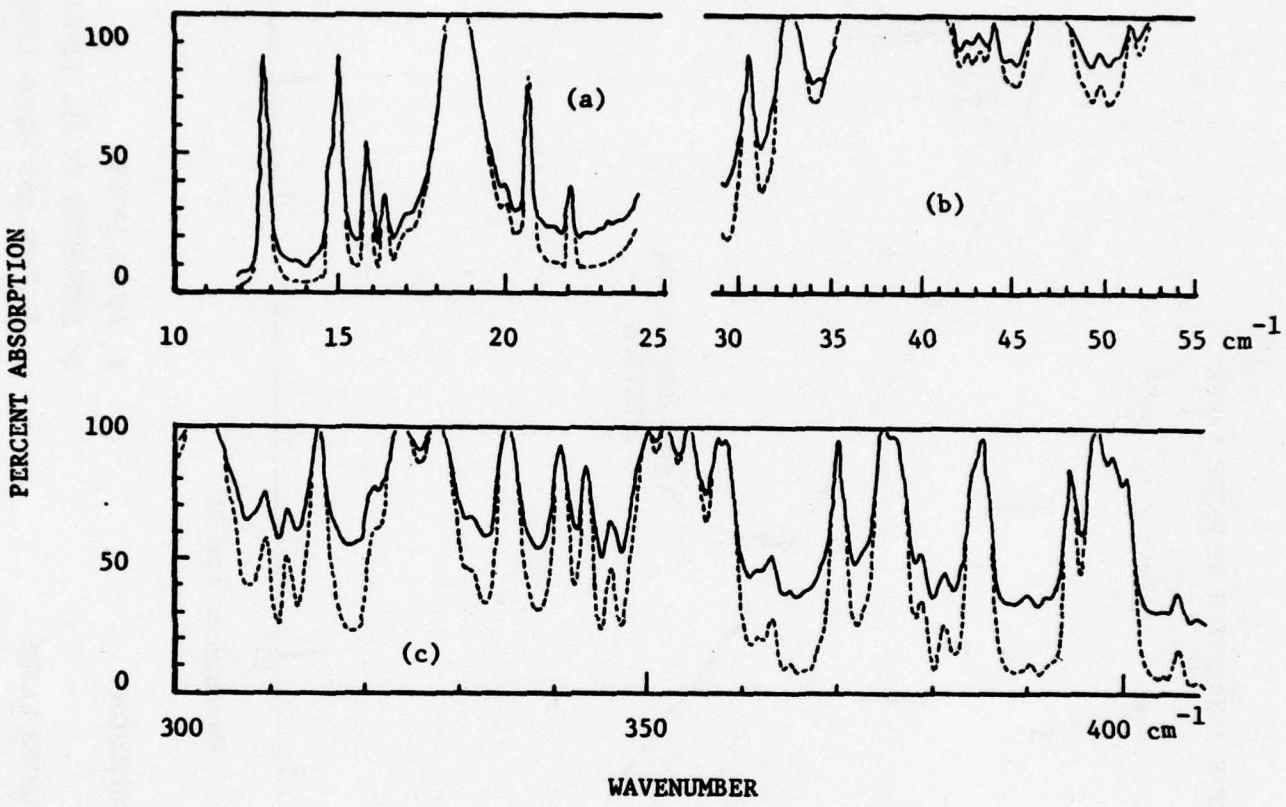

	WATER DENSITY $g\ m^{-3}$	TEMPERATURE K	PATH LENGTH m	RESOLUTION cm^{-1}	UNCERTAINTIES IN PERCENTAGE ABSORPTION
(a)	17	294	45	0.23	$\pm$1.25
(b)	15	294	103	0.5	$\pm$ 7 <40 cm^{-1} $\pm$ 1.6 >40 cm^{-1}
(c)	8.6	283	133	1.25	$\pm$2

Figure 3

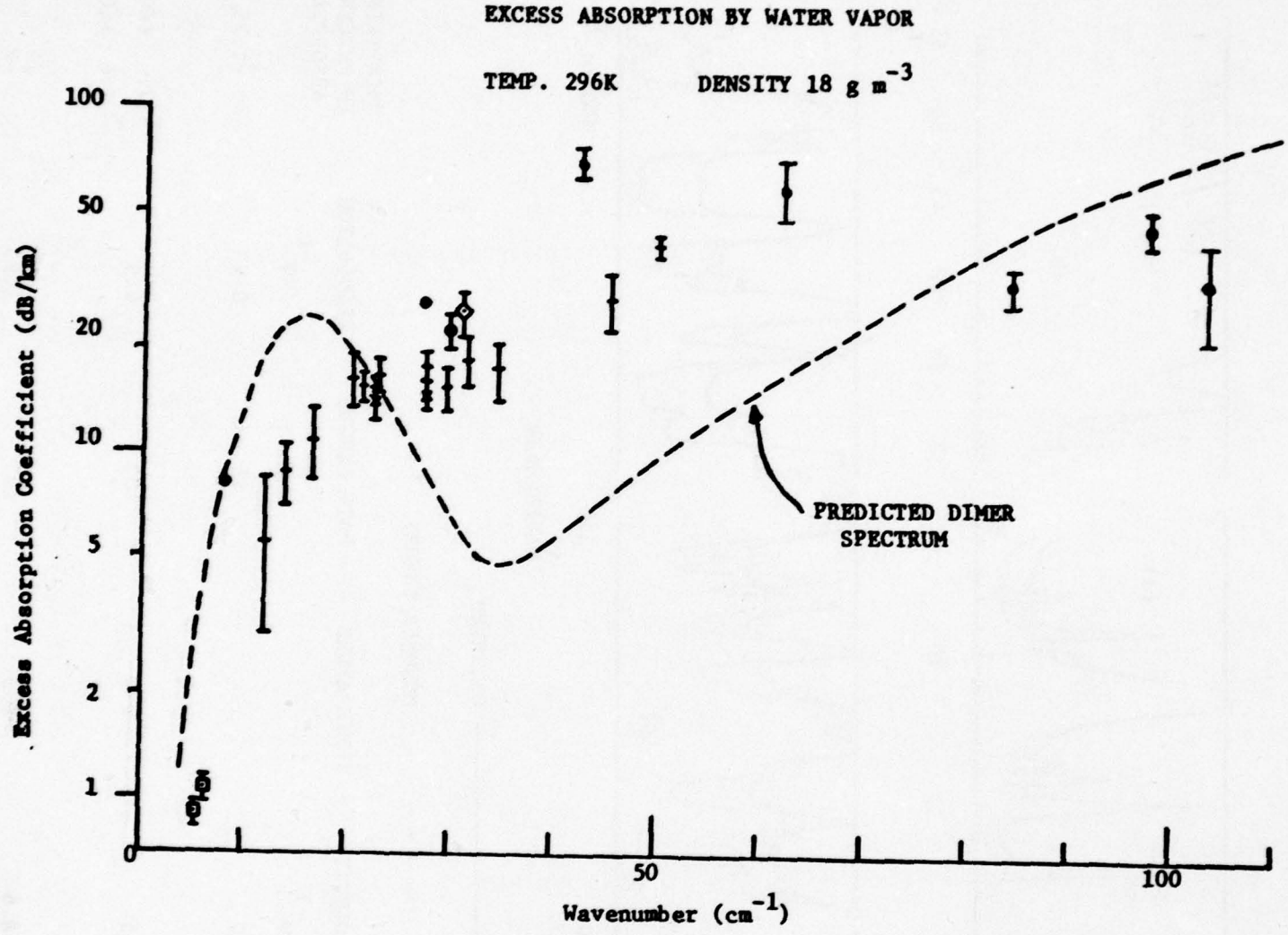
EXCESS ABSORPTION BY WATER VAPOR
TEMP. 296K DENSITY 18 g m^{-3}
Excess Absorption Coefficient (dB/km)
100
50
20
10
5
2
1
0
50
100
Wavenumber (cm^{-1})
PREDICTED DIMER SPECTRUM
H$_2$O
PRESENT OBSERVATIONS: + FOURIER SPECTROSCOPY
o HCN MASER
● OPTICALLY PUMPED LASER
X BURCH (1968)
◇ BURROUGHS ET AL. (1969)
□ FRENKEL AND WOODS (1966)

Figure 4

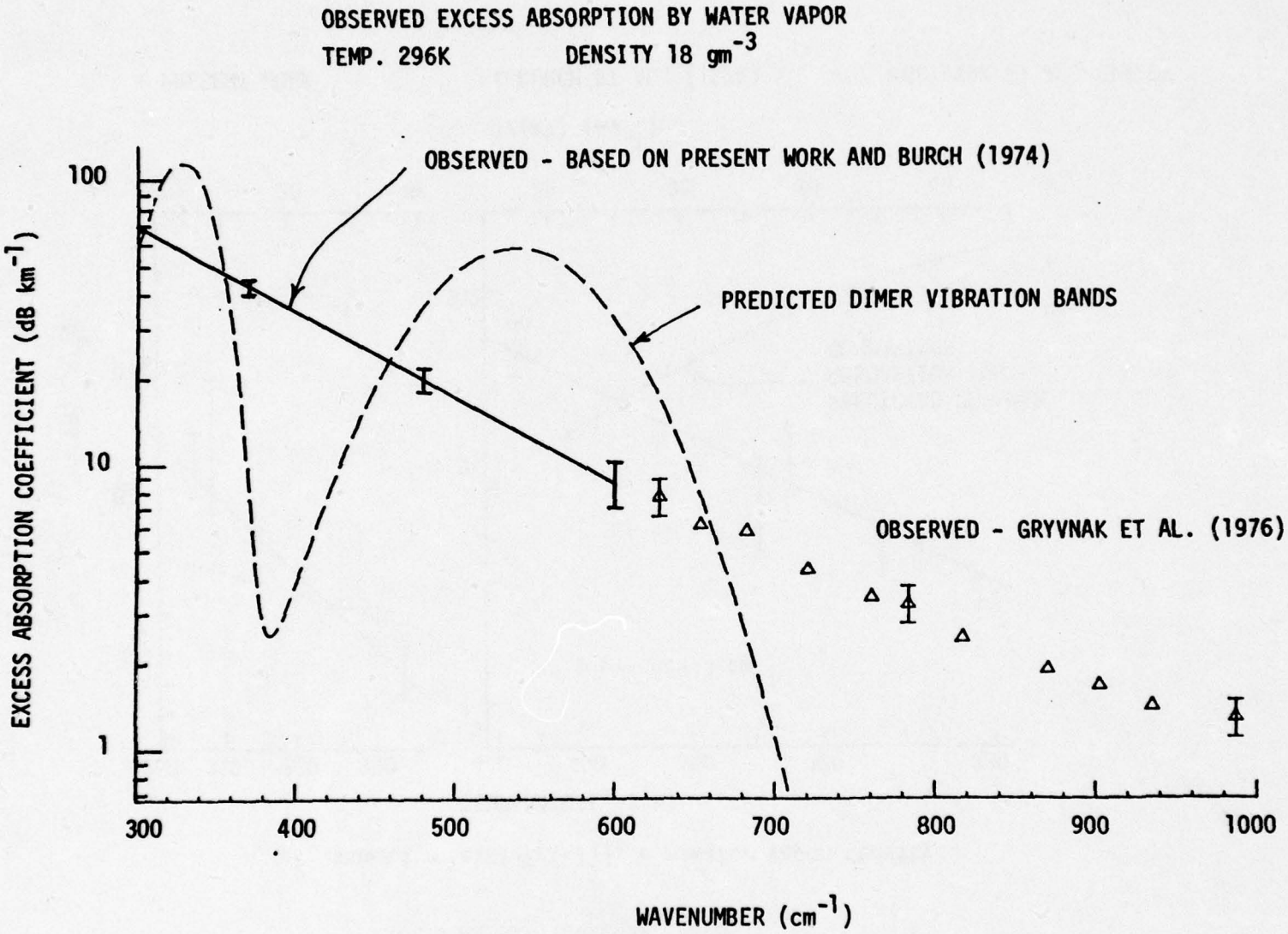
OBSERVED EXCESS ABSORPTION BY WATER VAPOR
TEMP. 296K DENSITY 18 gm^{-3}
OBSERVED - BASED ON PRESENT WORK AND BURCH (1974)
PREDICTED DIMER VIBRATION BANDS
OBSERVED - GRYVNAK ET AL. (1976)
EXCESS ABSORPTION COEFFICIENT (dB km^{-1})
100
10
1
300
400
500
600
700
800
900
1000
WAVENUMBER (cm^{-1})

Figure 5

OBSERVED TEMPERATURE DEPENDENCE OF THE
EXCESS ABSORPTION COEFFICIENT K_e

K_e/ρ^2 assumed $\propto$ exp[-E/(kT)], ρ = water vapor density

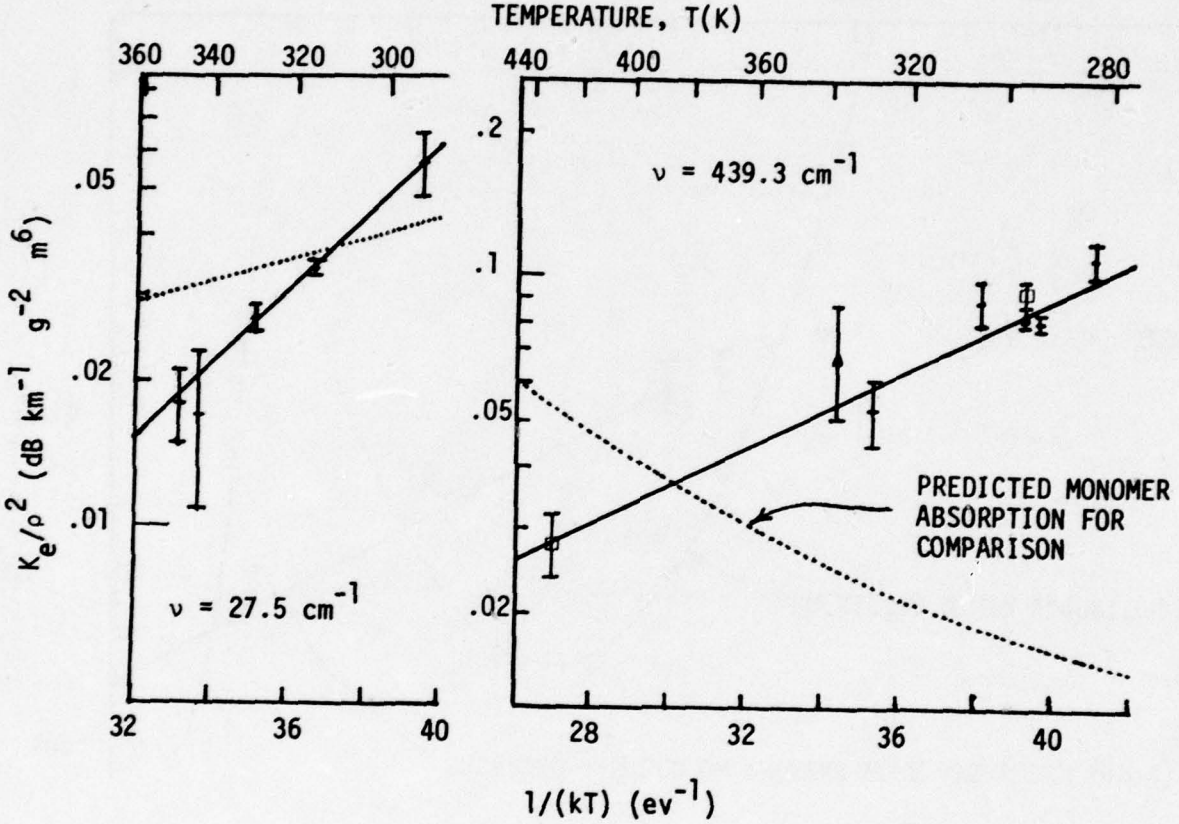

+ PRESENT WORK

□ BURCH ET AL. (1974)

▲ GRYVNAK ET AL. (1976)

Figure 6

ENERGY CHARACTERIZING OBSERVED TEMPERATURE DEPENDENCE
OF EXCESS ABSORPTION

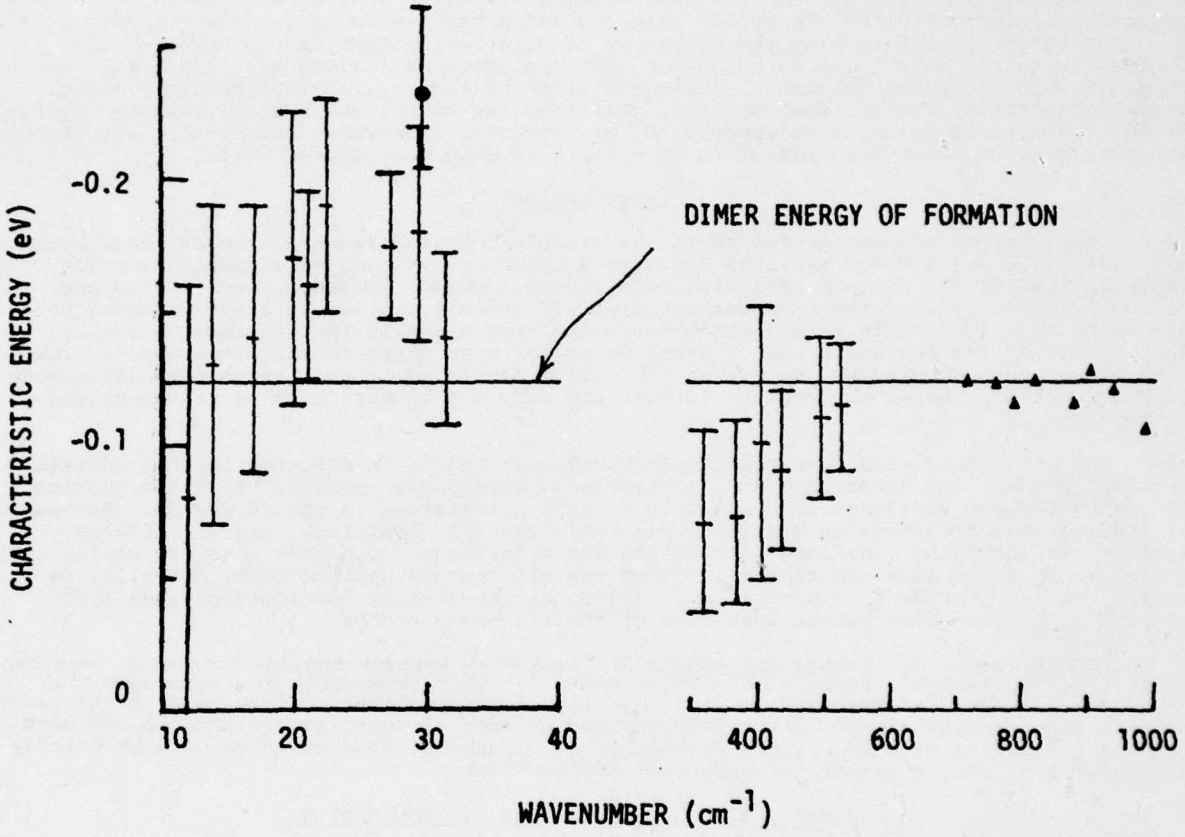

PRESENT WORK + FOURIER TRANSFORM SPECTROSCOPY

● MASER

GRYVNAK ET AL. (1976) ▲

Figure 7

PRESENTED AT 1979 IRIS CONFERENCE AND THE 23rd ANNUAL SPIE CONFERENCE, SAN DIEGO, CA., 27-31 AUGUST, 1979.

Military systems applications at near-millimeter wavelengths

J. J. Gallagher, R. W. McMillan and R. G. Shackelford

Engineering Experiment Station, Georgia Institute of Technology
Atlanta, Georgia 30332

Abstract

The near-millimeter wavelength region (3.2mm - 0.3mm) is being investigated for military systems applications during adverse weather and in the presence of smokes, dust and other particulate clouds. The use of near-millimeter wavelengths (NMMW) has advantages and disadvantages relative to the use of the infrared and microwave regions. The atmosphere is a dominant factor in determining the operation of military systems in the NMMW region. Systems currently under consideration for NMMW applications include beam rider and command guidance, missile plume detectors, low-angle tracking radars, terminal homing systems, target acquisition radars, fuze systems, quasi-imaging radars and hybrid (IR/NMMW) systems. Recent NMMW technological developments (e. g., sources, receivers, components, phenomenology and measurements) have been advancing at a rapid pace to meet system needs.

Introduction

Weapon guidance systems operating in the visible/infrared spectral regions have been successfully developed for tactical use over a broad spectrum of engagement scenarios. These include direct systems employing beam riders, command guidance, semi-active and active guidance modes which have demonstrated effective operation in clear weather, but are inoperable in certain severe atmospheric conditions and in the presence of smokes, dust and other particulate clouds. Since molecular absorption in the atmosphere is low over broad spectral windows throughout the visible/infrared, the primary attenuation mode is Mie scattering by water droplets in haze and fog, and by particulates in smokes and other aerosols.

On the other hand, the near-millimeter wavelength region is affected less by adverse weather, smokes, and aerosols than the visible/IR wavelength regions. Rain attenuation of NMM wavelength radiation is comparable to rain attenuation in the IR region. Because of its improved transmission under adverse environmental conditions, near-millimeter wavelengths are being considered for military applications. The NMMW spectral region will not prove to be an ideal operational region for all systems applications, but will, in several cases, provide a compromise adverse weather capability for limited range applications with resolution better than that of the microwave region.

In recent years, millimeter and near-millimeter wave systems applications have been the subjects of workshops[1], reports[2] and study panels[3]. This paper will draw upon material presented in these references, with the majority of information originating from the Harry Diamond Laboratories study[3]. A primary purpose of many of these investigations has been the identification of NMMW systems technology requirements, some of which will be briefly discussed following a summary of potential applications.

Advantages and disadvantages of NMMW region

The near-millimeter wavelength region has usually been dismissed in the past as a region of high attenuation, relative to the microwave region, and as a region of poor angular resolution relative to the visible/IR wavelength regions. However, several factors enter into the evaluation of the wavelength region which is chosen for operation of a particular system during adverse weather. It will be seen in the next section that transmission in adverse weather improves considerably in going from visible/IR wavelengths to NMM/MM wavelengths, and further improves at centimeter wavelengths. On the basis of this comparison, it would appear that centimeter or longer wavelengths would be the most appropriate for systems operation in adverse weather. Moreover, it has been shown that transmission through smokes and aerosols also follows a pattern of decreasing with increasing wavelength. Aimpoint accuracy requirements, however, tend to eliminate the centimeter wavelength region on the basis of a number of practical considerations. For example, the required accuracy for target tracking or target designation usually falls within the range of 0.1 to 0.5 mrad resulting in antenna dimensions of about 0.5 to 1 m for millimeter wavelengths and 5 to 10 meters for centimeter wavelengths. This consideration alone rules out a centimeter wavelength system for applications where the weapon system platform would be vehicle- or helicopter-mounted. Analysis of NMMW systems requires then that several factors be weighed in determining their potential in currently conceived tactical applications. Tables 1 - 4 list advantages and disadvantages of the NMMW spectral region relative to microwave and

infrared wavelengths. Some of the listed advantages might be questioned; thus, whereas the best of RF and optical techniques can be combined at NMM wavelengths, this can also be considered a necessity because of the nature of the spectral region. On the other hand, disadvantages such as component deficiencies and lack of data will be reduced or removed as work progresses at NMM wavelengths.

Whereas several of the NMMW disadvantages can be expected to diminish, the limiting factor for systems applications is the atmospheric effect, which cannot be avoided. The factor $e^{-\alpha R}$, where α is the atmospheric attenuation and R is the weapon-target range, is present in all propagation expressions. In the analysis and discussions of NMMW systems, their performance is dominated by their capability to operate under various atmospheric conditions. Since the major role for NMMW tactical systems will be during inclement weather or in the presence of smoke, the characteristics of a NMMW system, when such conditions prevail, are extremely important.

Table 1. Advantages for NMMW Region Relative to Microwave Region

1. Greater Resolution
2. Smaller Beam Angle θ_B for Given Antenna Diameter, D, and Conversely Smaller D for Given θ_B
3. Reduced Multipath Potentially Improved Low-Angle Tracking
4. Low Off-axis Detectability Providing High Security
5. Covertness Due to Exponential Fall-off With Range in High Attenuation Regions
6. Tracking Through Plumes Improved Over Microwave Systems
7. Smaller Components Allowing More Compact On-board Missile Systems
8. Clutter More Diffuse, Doppler Shift is Greater, Glint Should be Less
9. Integration of Hybrid IR/NMMW Systems Possible
10. Countermeasures More Difficult

Table 2. Advantages for NMMW Region Relative to Optical Region

1. Improved Transmission in Smoke and Fog, Providing Better Low Visibility Operation
2. Harder to Jam; More Covert
3. Improved Eye Safety
4. Better Coherent Receiver Techniques
5. Source Stabilization More Easily Performed
6. Potentially Lower Cost
7. Reduced Background
8. Both RF and Optical Technology Applicable

Table 3. Disadvantages for NMMW Region Relative to Microwave Region

1. Poor Heavy Rain Transmission
2. Atmospheric (clear) Absorption is Higher
3. Larger Rain Backscatter
4. Current Receiver Noise Figures are Poorer
5. Higher Precision Manufacturing Required
6. Solid State Source Efficiencies Fall as Frequency Squared
7. Poorer Source Stability
8. Inferior Waveguide Power Handling Capability
9. Higher Cost for NMMW Systems

Table 4. Disadvantages for NMMW Region Relative to Optical Region

1. Lower Resolution
2. Higher Glint
3. Lack of Relevant Data
4. Video Detection Less Sensitive
5. Component Technology Currently Worse
6. NMMW Laser Sources Less Efficient
7. Solid State and Tube Sources Chirped, Less Monochromatic Than Optical Lasers
8. Components Currently Larger and Heavier

Atmospheric effects

Whereas the NMMW region offers an advantage over optical systems during adverse weather, clear weather NMMW propagation suffers greater attenuation than experienced in the IR/visible region, and is, in addition, for most systems restricted to spectral windows. The NMMW region has strong O_2 and H_2O absorption lines with water the major absorber. Between these broad lines lie the transmission windows. Figure 1 shows the horizontal attenuation across the NMMW region from 100 GHz to 1000 GHz at sea level and 4 km altitude[4]. Also shown is the weak O_2 absorption at sea level. Because of the strong absorption at the

short wavelength end of this spectral region, tactical ground-to-ground or ground-to-air applications are confined to the longer wavelength windows which are centered about the following wavelengths:

Wavelength (mm)	Horizontal Attenuation (dB/km)	Zenith Attenuation (dB)
3	0.3	1.25
2.1	0.5	0.91
1.3	1.75	2.1
0.88	9.0	9.9
0.72	17	22

Included in this listing are approximate horizontal attenuation (dB/km) for 5.91 g/m^3 of H_2O at sea level and the zenith attenuation (dB) for 7.5 g/m^3 of H_2O at sea level. A more comprehensive indication of the horizontal attenuation across the electromagnetic spectrum (3 cm - 0.3 μm) is given in Figure 2. A clear air curve for H_2O density of

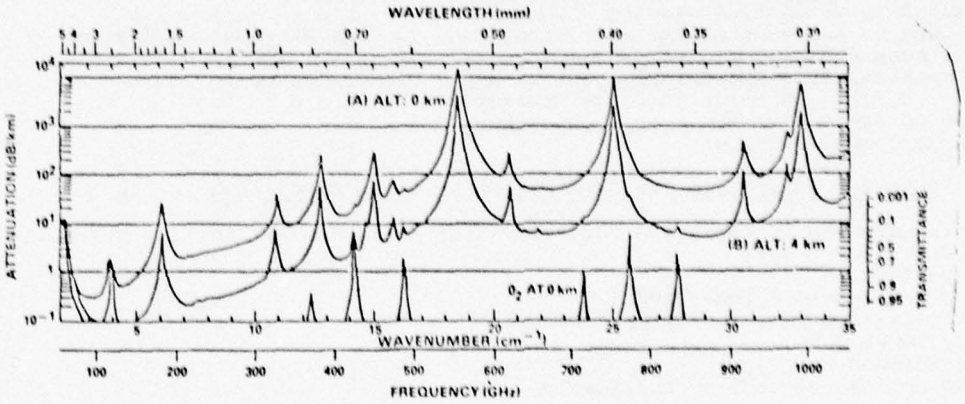

Figure 1. Spectral plots of the attenuation by the (1962) U.S. Standard Atmosphere at sea level and 4 km altitude. The water vapor density is 5.91 g/m^3 at sea level and 1.10 g/m^3 at 4 km altitude. The lower curve represents O_2 only at sea level. For comparison, the attenuation for this same model atmosphere is approximately 0.2 dB/km in the 10 micrometer window and less than 0.1 dB/km near 3.8 micrometers[4].

7.5 g/m^3 at 20°C shows the high attenuation in the submillimeter region surrounded by the low microwave and IR/visible attenuation. From the fog and rain curves of Figure 2, the

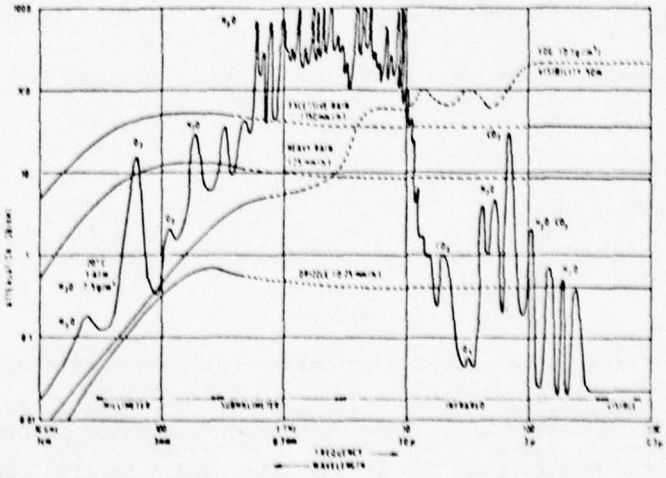

Figure 2. Attenuation by atmospheric gases, rain and fog[5].

advantage of NMMW systems during heavy fog and the comparable NMMW and IR attenuation during rain are demonstrated. A similar figure[6], Figure 3, shown increasing attenuation for clouds with decreasing wavelength, indicating an advantage for satellite or aircraft-to-ground sys-

tems applications. Near millimeter wave attenuation by aerosols is highly dependent on the

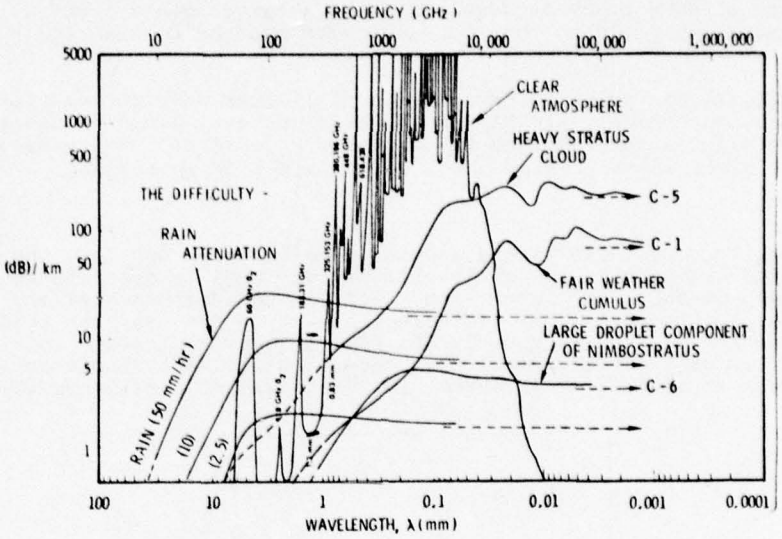

Figure 3. Summary of sea-level atmospheric attenuation[6].

type of aerosol and its particle size distribution and concentration. Table 5 shows the size range and concentration of water droplets in rain, fog and clouds. It can be seen from this table that the larger size range of rain droplets (7-700 μm) would cause significant scattering losses at near millimeter wavelengths were its concentration not extremely low compared to the concentration of water droplets in fogs and clouds. For both rain and fog, the attenuation is an almost linear function of bulk water density with the frequency dependence for attenuation in rain being negligible over the NMM spectral region from 94 to 340 GHz.

Table 5. Comparative Water Droplet Size and Density For Rain, Fog, and Clouds [8, 9, 10]

Rain				
	Light (r = 1 mm/hr)	Moderate (r = 4 mm/hr)	Heavy (r = 25 mm/hr)	Cloudburst (r = 100 mm/hr)
Size Range (μm)	7 - 100	10 - 300	10 - 500	50 - 700
Droplet Density (m^{-3})	350	500	700	1,250
Water Density (g/m^3)	0.04	0.17	1.0	4.2

Fog		
	Thin (vis. ~ 300 m)	Thick (vis. ~ 50 m)
Size Range (μm)	< 0.1	0.02 - 0.2
Droplet Density (m^{-3})	2×10^{10}	3×10^{11}
Water Density (g/m^3)	0.023	0.35

Clouds				
	Cumulonimbus	Cumulus Congestus	Fair Weather Cumulus	Strato Cumulus
Size Range (μm)	-	8 - 12	3 - 5	2 - 4
Droplet Density (m^{-3})	-	-	1.6×10^8	3×10^8
Water Density (g/m^3)	6.0	2.5	0.5	0.2

For aerosols resulting from smokes, dust or other battlefield-generated debris, the attenuation is primarily due to scattering, and secondarily to absorption. Preliminary indications[7] are that propagation through existing screening smokes is very high, and that the development of effective smokes for the NMMW region is questionable because of the difficulties involved with generating and dispensing smokes with the appropriate particle size distribution and settling rate. Attenuation of millimeter radiation by ground ex-

plosions of munitions has been shown to be relatively high for short periods of time[7]. Although the attenuation cleared much faster for NMM waves than for the IR/optical bands, nevertheless, loss of NMMW track or acquisition of a target could occur during a barrage or critically placed explosion so that these effects must be considered in greater detail in the future.

It is important at this point to demonstrate millimeter wave propagation under conditions of high absolute humidity and high bulk water content, since these are the conditions under which all military systems are expected to operate. Examples are given for the three cases: clear weather (high absolute humidity), rain and fog.

Clear weather

In high visibility conditions with a lack of precipitation and fog, the attenuation of near millimeter radiation in dB/km is directly proportional to absolute humidity. This linear relationship is shown in Figure 4 on a plot of temperature-humidity data which was abstracted from a psychrometric chart. Table 6 shows the two-way path loss for a range of 3 km at frequencies of 94, 140 and 220 GHz for various atmospheric conditions. Note that the attenuation of 220 GHz radiation is very high for warm, humid conditions although the total path loss is only 18 dB (3 dB/km) for the standard atmosphere (T = 300°K, ρ = 7.5 g/m^3).

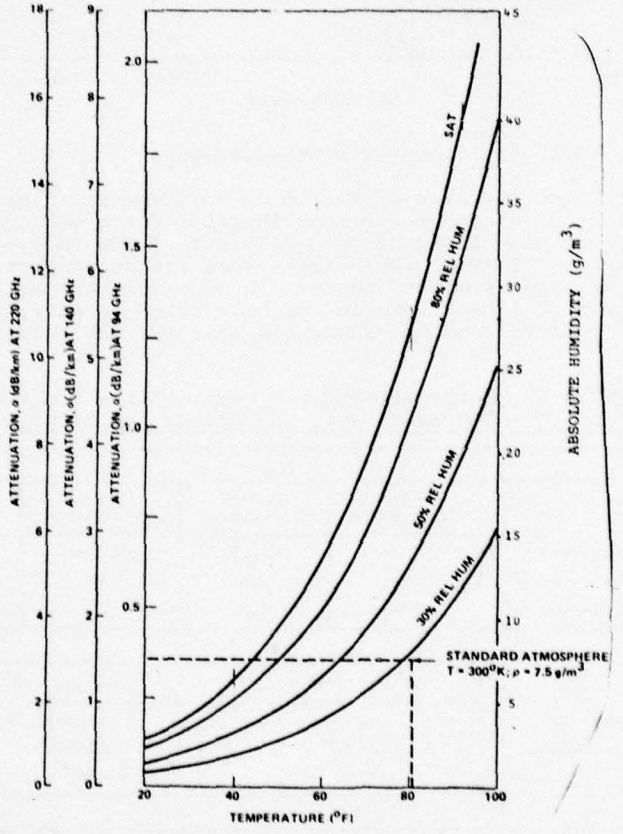

Figure 4. Atmospheric absorption by water vapor.

Table 6. Two-Way Path Loss In dB For Atmospheric Attenuation Over A Range of 3 km

Frequency (GHz)	Relative Humidity =	T = 90°F			T = 65°F			T = 40°F		
		30%	50%	80%	30%	50%	80%	30%	50%	80%
94		3.1	5.2	8.4	1.4	1.9	3.0	0.5	0.9	1.4
140		13.2	21.9	35.4	5.7	9.3	15.0	2.7	3.3	6.2
220		26.4	43.8	70.8	11.4	18.6	30.0	4.5	6.5	12.3

The impact of these attenuation figures on system design can be shown by solving the radar equation for a typical set of system parameters; the radar range equation is of the form

$$S/N = \frac{P_p \tau G^2 \lambda^2 \sigma_T}{(4\pi)^3 R^4 K T N_f L_T} \qquad (1)$$

where P_p = peak power of the transmitter; τ = pulse width of the transmitter (it has been assumed that the receiver bandwidth = $1/\tau$); G = gain of the transmitting/receiving antenna; λ = free space wavelength; σ_T = radar cross section of the target; R = range to target; K = Boltzmann's constant; N_f = noise figure of the receiver, and L_T = total radar system loss (atmospheric & signal processing + waveguide and components).

Assuming the following parameters:

τ = 200 nsec.; λ = 1.3 mm (230 GHz); G = 47.6 dB (6" aperture with η = 0.5); σ_T = 50 m^2; KT = 4.14 x 10^{-21} (T = 300°K); L_s = signal processing loss = 3 dB; L_w = waveguide and component loss = 8 dB; N_f = 12 dB.

we may write

$$S/N(dB) = P_T(dBW) - 40 \log R(km) - 2\alpha(dB/km)R(km) + 15.2$$

Figures 5 and 6 show S/N vs R for different values of P_T for atmospheric conditions of T = 27°C and ρ = 7.5 g/m^3 (standard atmosphere) and T = 30°C and ρ = 28 g/m^3 (relative humidity ≈ 80%). For these two cases, Table 7 shows the peak power versus range required for S/N = 14 dB (P_d = 0.9, P_{fa} = 10^{-7}). Note that for large α, the S/N vs R curves are very steep, and only small changes in range occur for large changes in P_T at a given S/N. With a maximum peak power of 10 kW, for example, the high visibility range will be limited to about 1.5 km on a warm humid day, and to about 3 km on a warm dry day. These calculations are for single pulse transmission only.

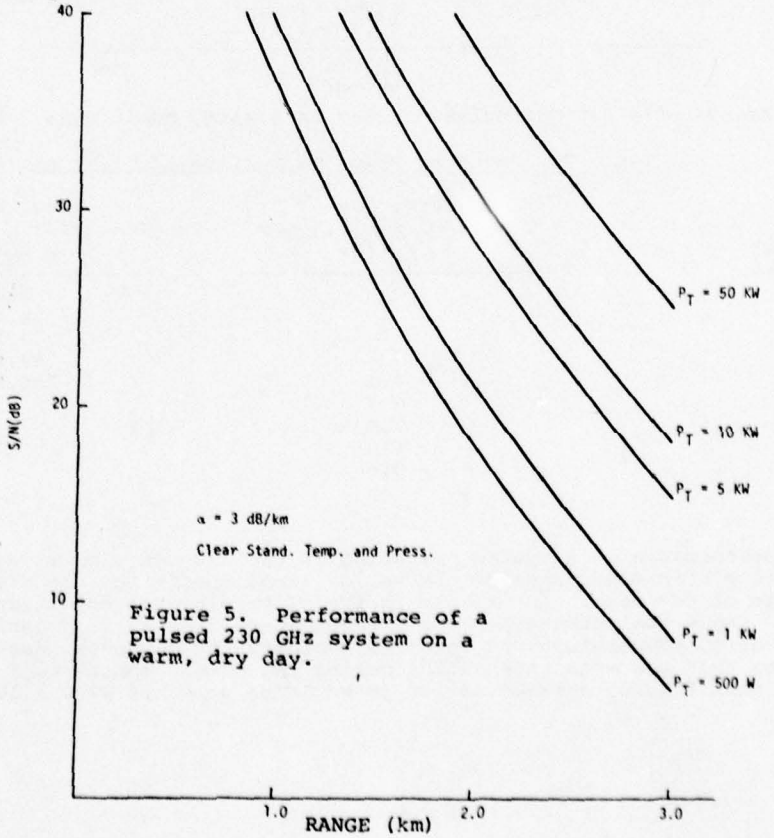

Figure 5. Performance of a pulsed 230 GHz system on a warm, dry day.

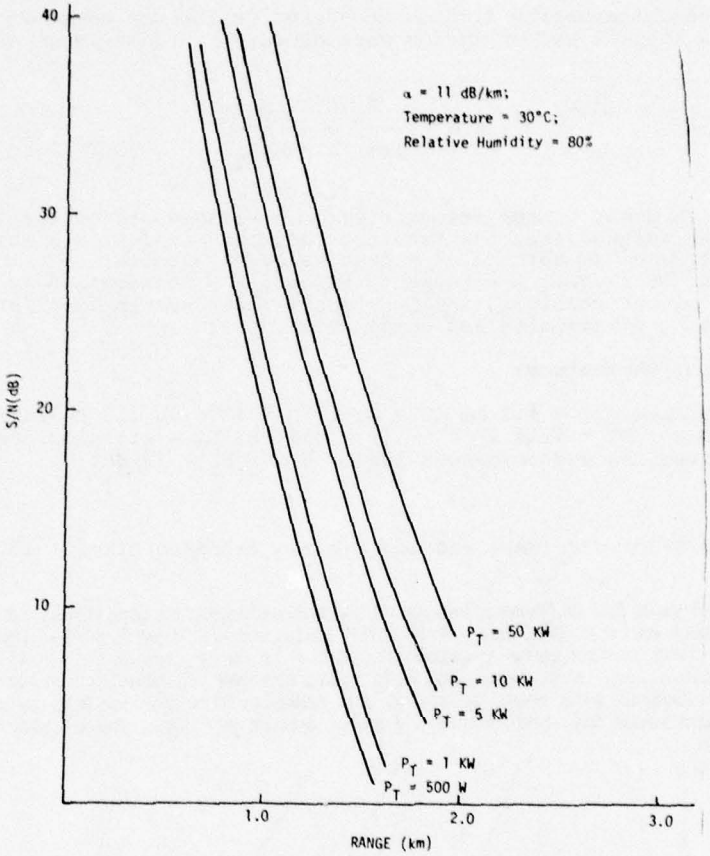

Figure 6. Performance of a 230 GHz pulsed system on a warm, humid day.

Table 7. Required Power To Achieve S/N = 14 dB

Range (km)	Warm, Dry T = 27°C, ρ = 7.5 g/m^3 P_T(KW)	Warm, Humid T = 30°C, ρ = 28.0 g/m^3 P_T(KW)
1.0		0.1
1.25		1.0
1.5		7.2
1.75		47.0
2.0	0.2	284.5
2.25	0.4	
2.5	0.9	
2.75	1.8	
3.0	3.6	

Although the performance of a system operating in the 230 GHz window degrades rapidly in warm humid weather, in many parts of the world these conditions are present for only a small percentage of the time. An example is the climatological conditions of Western Europe. Figure 7 shows the attenuation for three near-millimeter frequencies based on the mean maximum daily temperature and relative humidity for Bayreuth, West Germany. These data predict that the mean attenuation during the summer months will be less than 7 dB/km, and for this figure, a range of 2.0 km would be possible with a 10 kW pulse source.

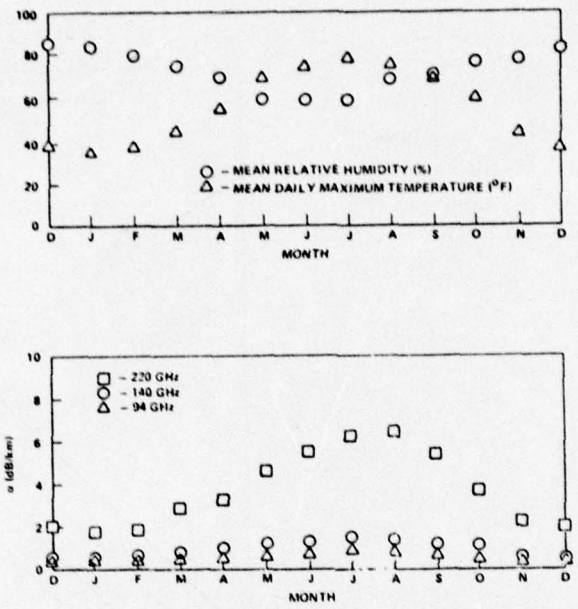

Figure 7. Millimeter wave atmospheric absorption by water vapor - Bayreuth, West Germany.

Rain. Although differences exist in predicted rain attenuation for the NMMW region[11], most models predict the following relationships:

$$\alpha(\text{dB/km}) = Ar^B, \tag{2}$$

where A and B are constants for the frequency region 94 - 340 GHz, and r is the rain rate in millimeters per hour. Based on the available data, the relation

$$\alpha(\text{dB/km}) \approx r^{0.85} \tag{3}$$

provides a reasonably close fit throughout the NMMW spectrum. As might be expected, a warm rainy day will be a problem for a system at 220 GHz because of strong absorption by both water vapor and bulk water. For example at T = 26.7°C (80°F), and r = 4 mm/hr. (a moderate rain rate), the attenuation is 11 dB/km (water vapor) plus 3 dB/km (rain) or 14 dB/km total. Figure 8 shows the S/N versus range at three power levels, and again it is evident that for a given value of S/N, large increases in power result in small increases in range. For this atmospheric condition, a peak power level of about 50 kW would be required for a range of 1.5 km at S/N = 14 dB whereas a range of about 1.2 km would be possible at the same value of S/N with only 5 kW peak power. An order of magnitude increase in power only results in about 0.3 km increase in range for this condition.

Fog. Attenuation of NMMW radiation by fog is also dominated by bulk water absorption, although a slight frequency dependence is also present. A good fit to available fog attenuation data is provided by the expression

$$\alpha(\text{dB/km}) = 0.035\ \rho(\text{g/m}^3)\ f^{1.08}(\text{GHz}) \tag{4}$$

This relationship along with the optical visibility is shown in Figure 9. For a 30 meter visibility radiation fog, with liquid water content of 0.75 g/m^3, the attenuation by water absorption at 230 GHz is approximately 9 dB/km. As shown in Figure 7, the mean maximum daily temperature of Bayreuth, West Germany during the winter months (the season of greatest incidence of fog) is about 0-4°C; therefore a reasonable fog scenario is 30-100 m visibility with temperature 0-4°C, for which the attenuation at 230 GHz would be approximately 4 dB/km to 11.5 dB/km. These conditions have been bracketed by the calculations presented in Figures 5 and 8. It is significant to point out that a 100 m visibility fog at T = 4°C (40°F) results in an attenuation of only 4.5 dB/km at 230 GHz compared with about 50 dB/km in the 8-12 μm band and about 150 dB/km at a wavelength of 0.6 μm.

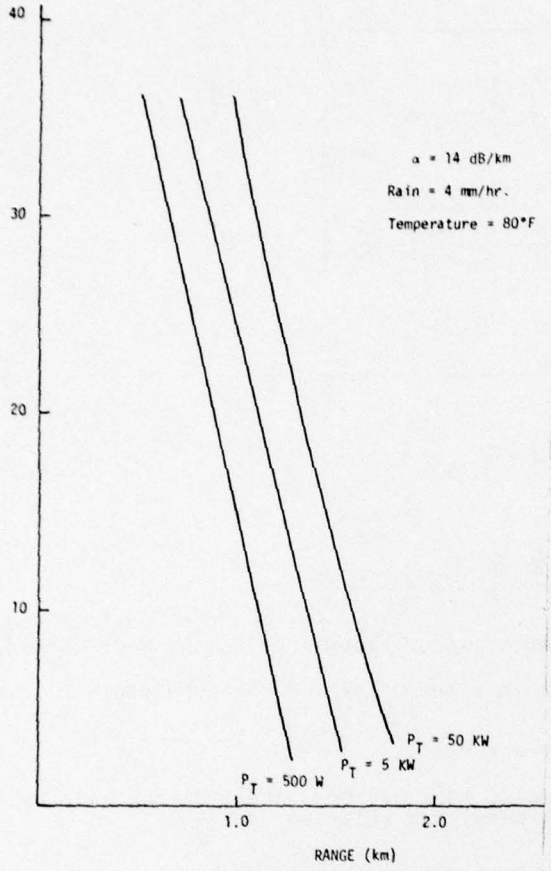

Figure 8. Performance of 230 GHz pulsed system in rain.

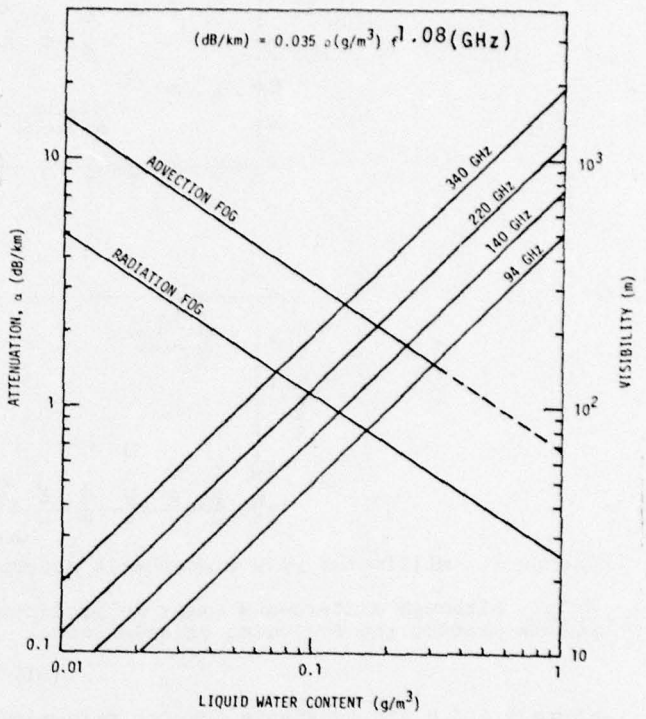

Figure 9. Millimeter wave attenuation by fog.

A summary of atmospheric propagation data, convenient for system calculations, is given in Table 8. The majority of information presented thus far has dealt with atmospheric effects appropriate to radar or communication applications. An equally important consideration is the influence of the atmosphere and environment on radiometric signals. When observing a target in its surroundings, it is important to know the brightness temperature contrast between target and other objects. This contrast is a function of frequency, the atmosphere, and target and background characteristics (reflectivity, emissivity, etc.). The antenna temperature of a radiometer looking downward from altitude h at an angle θ to the vertical is given by

$$T_B = \int_h^\infty T(z)\exp[-\tau(h,z,\theta)]\alpha(z)\sec\theta dz + R\exp[-\tau(o,h,\theta)]\int_h^\infty T(z)\exp[-\tau(z,o,\theta)]\alpha(z)\sec\theta dz + (1-R)T_E\exp[-\tau(o,h,\theta)]$$

where T_E is the temperature of the earth- or ground-based target and $T(z)$ is the temperature of a stratum of atmosphere of thickness dz located at altitude Z. The terms of the form $\tau(Z_1, Z_2, \theta)$ are the optical depths between altitudes Z_1 and Z_2 at angle θ, and R is the reflectivity of the earth or target. The optical depths τ are given by

Table 8. Summary Of Propagation Data

Attenuation, α (dB/km)
Water Density, ρ (g/m^3)

λ (μm)	α Clear Rel. Humidity = 100% T = 32°F ρ = 4.8	68°F 17.4	α Fog Radiative Fog R_V = 400m ρ = 0.014	200 0.038	100 0.11	30 0.71	α Fog Advection Fog 400 0.063	200 0.18	100 0.4	α Rain mm/hr 1	4	10	α Cloud Fair Weather Cum.	Nimbo-Strat.
1				80		500							95	570
4													120	640
10.6	0.3	1.2	7	20	58	373	17	63	140	1	2.6	6	50	500
337	50	185	0.6	1.5	4.3	28	2.5	7.1	15.8	1	3	7	3	20
724	10	37	0.3	0.9	2.6	17	1.0	4.3	9.6	1	3	7	2	7
880	7	24	0.3	0.7	2.0	14	1.2	3.5	7.9	1	3	7	1.5	6
1300	2	6	0.2	0.5	1.4	9	0.8	2.3	5.1	1	3	7	0.8	4
2300	1	3	0.1	0.2	0.6	4	0.4	1.0	2.2	1	3	8		2
3200	0.2	0.9	0.1	0.2	0.5	3.2	0.3	0.8	2	1	3	8		1.5

Notes: (1) for α_{CLEAR} at other Rel. Hum., scale down from 100% given

(2) for a fog situation, $\alpha_{TOTAL} = \alpha_{CLEAR}$ (RH = 100%) + α_F (likewise for clouds)

(3) for a rain situation, $\alpha_{TOTAL} = \alpha_{CLEAR}$ (RH = 100%) + α_R

$$\tau(Z_1, Z_2, \theta) = \int_{Z_1}^{Z_2} \alpha(Z) \sec \theta dZ \qquad (6)$$

so that the first term of Equation (5) is the contribution of the intervening atmosphere between the radiometer and target, the second term represents atmospheric emission reflected from the target to the radiometer, and the third term is the target's emission attenuated by the atmosphere between the radiometer and target. The target or earth background reflectivity is given by R, the target (earth) temperature is T_E and the atmospheric attenuation is $\alpha(Z,\nu)$. It is seen from these relations that not only atmospheric absorption by O_2 and H_2O is important, but hydrometeorite absorption and scattering and atmospheric thermal emission are also determining factors for the radiometric antenna temperature, which is reduced further in value when the target fill factor for the antenna is less than one.

Preissner[12] has shown the brightness temperature contrast for different weather conditions and different materials for the microwave through NMMW spectral region. Figure 10 demonstrates the brightness temperature contrast between vegetation and concrete for three different altitudes for a clear standard atmosphere (ρ_{H_2O} = 7.5 g/m^3, T = 20° C and P = 760 mmHg at sea level). At all altitudes given, a detectable brightness temperature contrast exists, except possibly at 230 GHz for 3 km and 8 km, where the temperature contrast is on the order of 3-5° K and the minimum detectable temperature is approximately 0.5-3° K for a 1 GHz bandwidth and a 10 msec time constant. Figure 11 shows the brightness temperature contrast (concrete and vegetation) for a radiometer at 3 km altitude for several atmospheric conditions. Rain severely degrades NMMW radiometric response and fog of visibility of 100 m or less results in considerable loss of contrast. A more significant indication of radiometric capability to detect a military target is the brightness temperature contrast for metal relative to vegetation. Figures 12a and 12b show contrasts for metal, water and concrete relative to vegetation. For metal, detectable contrasts are observed for all conditions except the 25 mm/hr rain. It must be emphasized, however, that, for metal, reflectivity of 1 has been used and no fill factor reduction has been employed. Both conditions are unlikely. Systems applications require further consider-

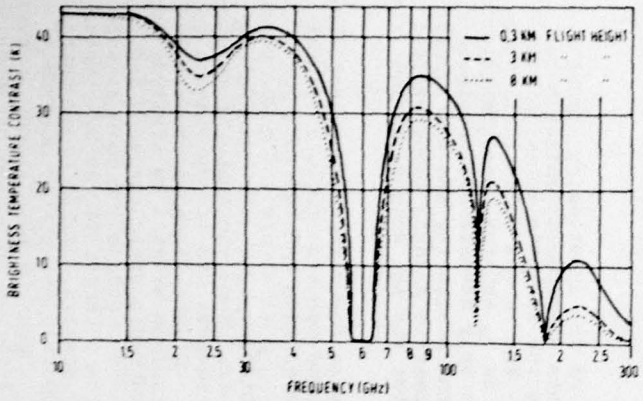

Figure 10. Brightness temperature contrast between vegetation and concrete for three different heights[12].

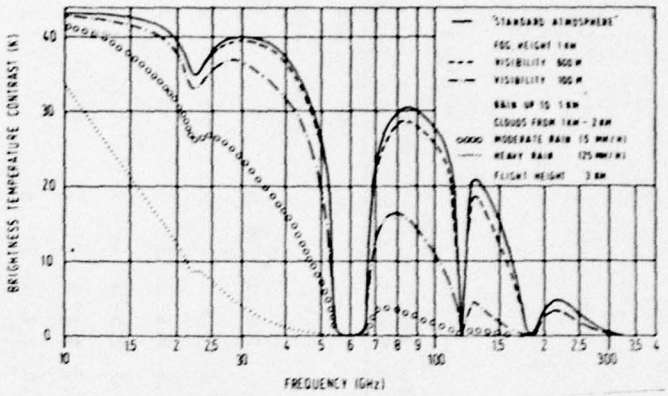

Figure 11. Brightness temperature contrast between vegetation and concrete for different weather conditions[12].

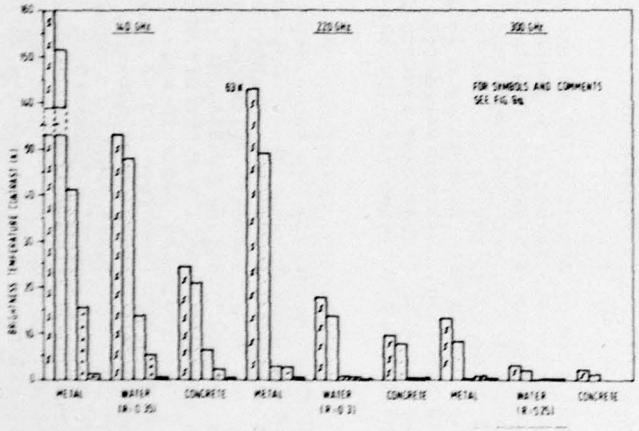

Figure 12a. Brightness temperature contrast for different objects, weather conditions and frequencies (11 GHz, 140 GHz, 90 GHz)[12].

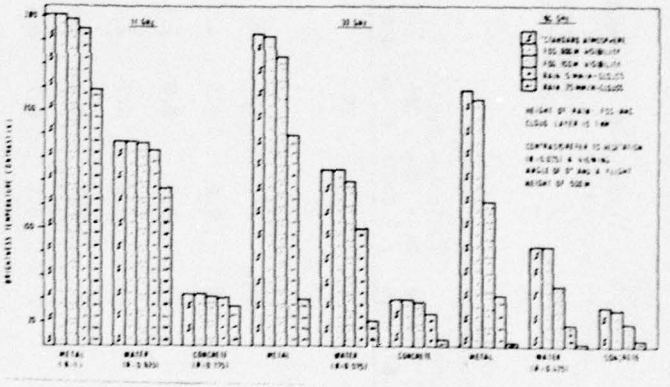

Figure 12b. Brightness temperature contrast for different objects, weather conditions and frequencies (140 GHz, 220 GHz, 300 GHz)[12].

ation of these effects with inclusion of antenna pattern and fill factor effects.

Very little data exist for atmospheric turbulence in the NMMW region; fluctuation of intensity and signal angle of arrival for NMMW systems have been studied by Armand et al.[13] and by Snider, Wiltse and McMillan[14]. Based on the approach first proposed by Armand, the peak-to-peak intensity fluctuations expected for a 230 GHz system under near standard conditions were calculated to be 1.16 dB, and the corresponding angle-of-arrival fluctuations were determined to be 0.3 mrad. In practice, observed intensity fluctuations at lower frequencies have occasionally been observed to be much larger, and little data are available for the angular fluctuations. Much work needs to be done before the effects of turbulence on NMMW systems have understood, but the meager results available to date indicate that it gives system degradation of a magnitude which must be considered.

The approximations discussed thus far demonstrate some of the atmospheric effects to be considered in systems trade-offs between the NMMW and IR/visible regions but do, in no way, describe the complexity that could occur at NMM wavelengths. Thus, when the limited experimental data for H_2O are compared with existing theories, the measured values in the window regions invariably exceed theoretical values. When measured values are compared with the monomer spectrum calculated with the Van Vleck-Weisskopf[15] or Gross[16] lineshape, the inadequacy of the theory is evident from Figure 13 in which the dashed curve B represents an empirical "continuum" absorption which must be added to bring the theoretical results into coincidence with the experimental results[4]. The empirical correction term has been given in the form[17]:

$$\Delta \alpha_{\nu} = 4.69 \times 10^{-6} \rho \left(\frac{300}{T}\right)^{2.1} \left(\frac{P}{1000}\right) \nu^2 \left(\frac{dB}{km}\right) \qquad (7)$$

where ρ is the water density (g/m^3), T is the atmospheric temperature, $^{\circ}K$, P is the pressure and ν the frequency. The discrepancy between measured and calculated water-vapor absorption closely follows this empirical correction term throughout the NMMW region. Various causes have been postulated for this excess or anomalous absorption, but, thus far, the source is not understood. Great anomalies have been observed in high humidity, cold conditions and in fog[18]. Further experimentation is needed in this area of atmospheric effects.

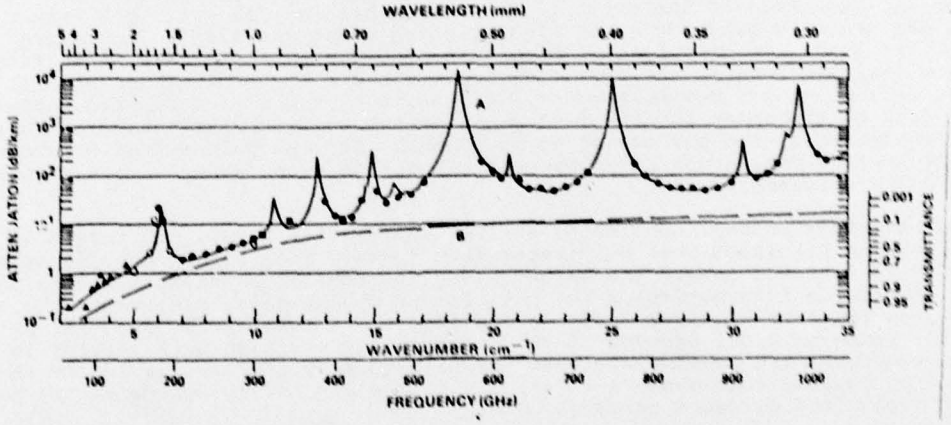

Figure 13. Spectral plots of the attenuation by atmospheric H_2O at sea level. Curve A represents a combination of theoretical and experimental results for an H_2O density of 5.91 g/m^3. At a fixed temperature and 1 atm total pressure, the attenuation is approximately proportional to the H_2O density. Curve B corresponds to an empirical continuum that is added to theoretical results to provide agreement with the experimental results. The transmittance scale on the right-hand side corresponds to a 1 km path[4].

Considerable space has been devoted in this paper to a discussion of atmospheric effects on propagation. However, it is just these effects which are the most important factors in determining the applicability of a particular military system in the NMM wavelength region.

Potential NMMW systems applications

Several NMMW military applications have been investigated in recent years. Of these, some have not shown advantages over the equivalent system operating in another spectral region, whereas some have sufficient promise to warrant initiation of experimental development of prototype systems. Among the potential systems applications which have been studied are the following[1-3]:

1. Beamrider systems
2. Terminal homing
3. Target designation and semi-active homing
4. Command guidance
5. Target surveillance and acquisition
6. Active NMMW quasi-imaging
7. Low angle tracking
8. IFF systems
9. Airborne passive imaging
10. Aircraft detection from satellites
11. Boost phase plume detection
12. Re-entry applications
13. Secure communications
14. Mine detection
15. Obstacle and terrain avoidance
16. Space object identification (SOI)
17. Fuzing
18. Hybrid (IR/NMMW) systems

The details of the investigation of most of these systems can be found in the references, and only a selected system, the NMMW beamrider, and brief statements on others will be discussed in this section.

Beamrider

A beamrider guidance system[19, 20, 21] is defined as a technique for guiding missiles which utilizes a beam directed into space, such that the beam axis forms a line along which it is desired to direct a missile. The missile contains equipment that can sense the direction and magnitude of the error when its path has deviated from the center of the beam, and that can generate guidance error signals which cause the missile to return toward the center of the beam. In principle, a beamrider system can be employed in surface-to-surface, surface-to-air, air-to-air, and air-to-surface roles, although it is potentially more effective against slowly moving targets. The basic elements of a beamrider system are the same for each of the roles but the stringency of the requirements placed on these elements will be determined by the particular applications. For the purposes of interest here, a surface-to-surface anti-armor role has been emphasized as an example of a credible application of NMMW guidance.

In the beamrider concept adopted as an example for this study, the target is acquired and tracked by a precision near millimeter wave (NMMW) radar with a conical scan antenna. The missile is launched toward the target along the conical scanning tracking beam, which is coded to provide information on the position of the missile relative to the scan axis which defines the line-of-sight (LOS) to the target. A receiver in the rear of the missile detects the scanning beam, decodes it to determine its position with respect to the scan axis, and generates the appropriate error signals to keep the missile in the center of the beam. In the conical scan mode, a relatively simple PRF coding scheme can be used to develop the required guidance error signals.

Figure 14 shows the NMMW beamrider guidance concept. The first and second beams are the capture beams which establish line-of-sight (LOS) guidance as quickly as possible. The basic functions of the beamrider system are target acquisition, target track, missile capture and missile guidance.

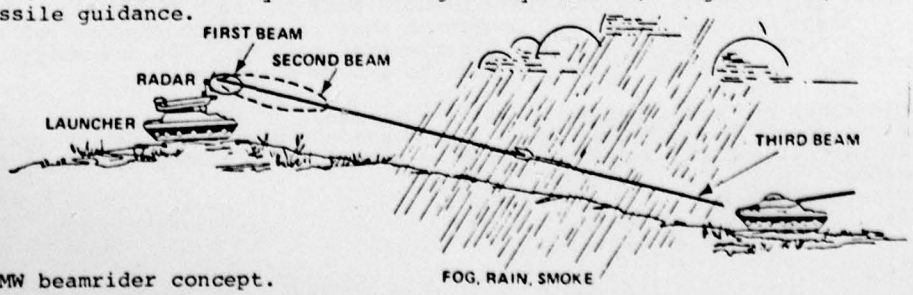

Figure 14. NMMW beamrider concept.

The basic system configuration considered to be most desirable for a ground-to-ground, anti-armor beamrider system requires that the entire system be a self-contained, crew-served and vehicle-mounted package with an antenna aperture diameter less than one meter. The candidate missile would be of the TOW or SHILLELAGH generic class, and would be tube-launched from the tracking/guidance platform. This concept would require an integrated target acquisition capability for performing target handover from a wide-area battlefield surveillance system, and for establishing an autonomous operating capability over a limited battlefield sector. The acquisition capability would of necessity require the development of suitable target recognition criteria based on the near millimeter wave target signature.

Nominal system parameters relating to these requirements have been given as the following[21]:

Operating Range	- Maximum: > 2 km; Minimum: < 0.5 km
Capture Range	- Maximum: $\leq$ 100 m
Weather and Environmental Extremes	- Rain: 4 mm/hr; Fog: 100 m vis. Temperature: 90 - 100°F; Relative Humidity: 80 - 100% Smoke: Battlefield-generated dust and aerosols; tactical screening agents
Acquisition	- Search Sector: 5° x 25°, movable scan sector; Search Time: < 10 sec.
Missile Data Rate	- 50 Hz

In addition to these characteristics, a NMMW system should also satisfy the general requirements of high reliability and maintainability, compatibility with existing equipment, capability for CM hardening, minimum operator interaction and training, rapid fire capability, and high first round probability of kill.

Based on these requirements, system concepts and estimated performance for a NMMW anti-armor beamrider system have been addressed[21]. However, the paucity of essential data for target and terrain reflectivity and atmospheric propagation may result in an altering of the performance calculations when those data become available.

The beamrider concept has been successfully implemented in the infrared, demonstrating good clear weather performance. Currently, there is an enthusiastic interest in the beamrider for the anti-armor application. The U. S. Army Ballistic Research Laboratory (BRL) has successfully carried out a feasibility demonstration of beamrider tracking and guidance at 140 GHz[20], and plans to repeat these experiments at 217 GHz. Efforts have also been initiated at U. S. Army MIRADCOM to define and verify a baseline beamrider missile system for anti-armor applications.

The critical performance parameters of any beamrider system are related to (1) high accuracy centroid tracking of the target, (2) a temporal and spatial beam structure such that the missile guidance is not biased by the terrain effects, and (3) a method of capturing the missile at a range close enough to insure adequate damping of the missile's angular deviations from LOS at the closest tactical range of interest.

The application of beamrider technology is most promising in the guided direct fire anti-tank role with the radar and launcher borne by a land vehicle. The system as presently envisioned requires a relatively large antenna ($\sim$ 0.6 m diameter), a precision tracking mount, and a dual beamwidth antenna configuration to accomplish missile capture. It is not feasible to consider a helicopter-borne weapon system at this time because of the size of the antenna/mount configuration; however, it may be possible to exploit optical scanning techniques which involve stabilization of scan components to obviate the requirement for a large precision tracking mount. The anti-helicopter role could be considered if the target exposure time is adequate to acquire and to accommodate the missile time-of-flight. In the anti-aircraft role the end game maneuverability requirements on the missile would be severe for crossing targets or for targets performing high G maneuvers; however, such a system appears to be feasible.

In considering why a beamrider system should be investigated as the initial concept for NMMW guidance feasibility rather than another scheme, the following factors are influential:

(1) The guidance link is one-way, so that relatively simple video receivers are potentially adequate for the missile link.

(2) Beamrider guidance has been demonstrated at IR and optical wavelengths in operational situations so that it is not necessary to go through a concept demonstration phase.

(3) Target cross section is high because the tracker looks at backscatter rather than at off-axis scatter.

(4) Since only the low cost missile receiver is expended in firing, the cost per round could be significantly less than that for a missile employing an active seeker.
(5) The missile is difficult to jam since the receiver looks back at friendly territory.
(6) It is possible to implement a multiple wavelength system so that wavelength optimization is possible for the acquisition, tracking and guidance functions.
(7) The airframe could be optimized aerodynamically since there is no seeker to complicate the warhead. Complexity of the on-board guidance and control is minimal.

The NMMW beamrider system must perform several functions in sequence, with the capability for continuity or rapid handover from one function to the next. This system must be capable of searching for and acquiring a target over a limited field-of-view (FOV), followed by the target tracking and missile guidance. Handover from the tracking to guidance modes must include a missile capture phase during which the missile is launched toward the target and LOS guidance along the tracking radar beam is established. For simplicity, it is desirable that one system at a single wavelength perform the entire beamrider operation; however, because of the complexity of these multiple operations (target acquisition, tracking, missile capture and guidance), the optimum configuration might require a multi-wavelength system.

Several approaches for implementation of the beamrider system have been investigated[21]. Performance in inclement weather is the most important consideration for a NMMW beamrider. For 94 GHz, 140 GHz and 220 GHz, an example of the transmitter power requirement for target acquisition as a function of range for rain rates of 4 and 16 mm/hr on a warm day is given in Figure 15. The following parameters are used in the calculations for source power:

	94 GHz	140 GHz	220 GHz
λ (m)	3.19×10^{-3}	2.14×10^{-3}	1.36×10^{-3}
G_T (dia. = 0.6 m; η = 0.5)	1.78×10^{5}	3.88×10^{5}	9.60×10^{5}
σ_T (m^2)	30	30	30
L_{RF}	0.5	0.40	0.16
S/N	3.1 (4.9 dB)	6.2 (7.9 dB)	38.9 (15.9 dB)
kTB (B = 10^7 Hz)	4.14×10^{-14}	4.14×10^{-14}	4.14×10^{-14}
N_f (dB)	4	7	15

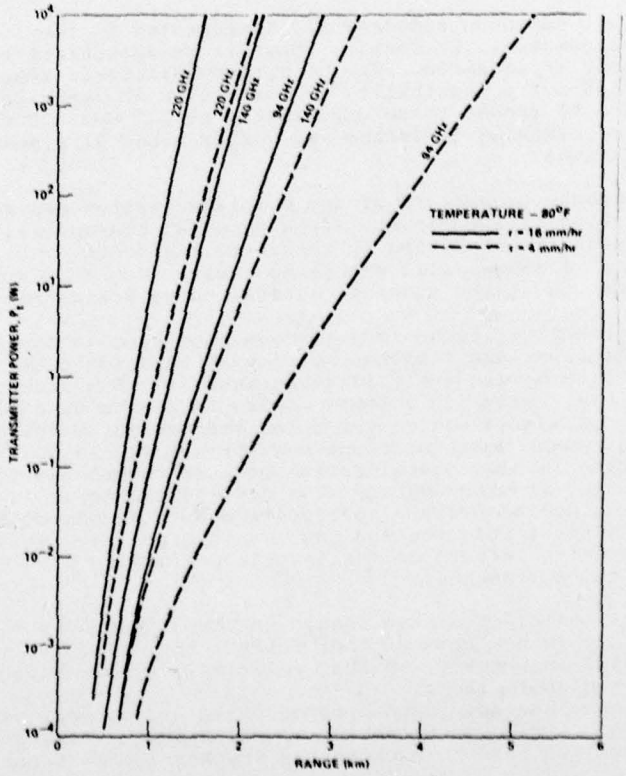

Figure 15. Power required for target acquisition on a warm day with moderate to heavy rain.

Trade-offs between search time, PRF, and antenna beamwidth must be considered in designing a beamrider system. If a separate acquisition system is employed, the required S/N for tracking will be considerably improved by the integration of additional pulses during the tracking interval which is long with respect to the acquisition target dwell time.

The curves of Figure 15 show that only the 94 GHz system is capable of a range of 3 km with a power of 1 kW in moderate rainfall. The transmitter power requirements for missile guidance are not as severe as those required for acquisition and tracking because the guidance link is a one-way path. It has been shown[21] that power levels required for acquisition are more than adequate for guidance.

For a five year projection of system performance, it would seem reasonable to anticipate improved noise figures and decreased RF losses at 140 and 220 GHz. These projections of improved performance are listed below:

Frequency (GHz)	State-of-the-art			5 Year Projection		
	L_{RF}	NEP	N_f	L_{RF}	NEP	N_f
140	4 dB	1.6×10^{-12}	7 dB	3 dB	10^{-12}	6 dB
220	8 dB	5×10^{-12}	15 dB	3 dB	10^{-12}	6 dB

The reason for projecting the same parameters for both frequencies is that quasi-optical components should show very little frequency dependence over the range, and the cutoff frequency of Schottky barrier mixers is presently about 3000 GHz.

Target acquisition, guidance with video detection and tracking have been calculated with the projected parameters. For tracking, it is assumed that the tracking error is

$$\sigma_m \approx \frac{CEP}{\sqrt{3R}} = \frac{0.35}{R(m)} ,$$

and a pulse integration gain of 17 dB is also assumed.

The projected performance levels for acquisition and tracking are shown in Figures 16 and 17 for each of the frequencies and a 1 kW source. Corresponding curves for guidance were not plotted because power adequate for the other two functions is more than adequate for guidance. These curves show some improvement over those of Figure 15; in particular, they show that it is possible to achieve tracking and guidance at a range of 3 km under more stringent conditions than before.

The calculations in the study show that, neglecting angle error due to multipath and glint, 94 GHz is the best frequency for a multifunctional tracking, acquisition and beamrider guidance system using state-of-the-art performance parameters. For a system dominated by multipath effects, either 140 or 220 GHz appears to be the preferred choice for operating frequency; whereas, without the presence of multipath effects, 94 GHz is a better choice for development of first generation millimeter guidance systems. This result is to be expected for performance dominated by propagation effects, since the absorption due to water vapor is much higher at 140 and 220 GHz than at 94 GHz. On the other hand, it would seem that tracking accuracy would favor 140 or 220 GHz in view of the reduced beam divergence at shorter wavelengths. For a conscan tracker, the tracking error due to thermal noise is $\propto \theta_B/\sqrt{S/N}$, and the $\sqrt{S/N}$ decreases faster than θ_B as the wavelength goes to 2.14 mm (140 GHz) and 1.36 mm (220 GHz) due to the increase in mixer noise figure and atmospheric attenuation coefficients at the shorter wavelengths. Even for projections based on extrapolation of available source power and improved performance of quasi-optical components, the 94 GHz window is still slightly preferable in terms of tracking accuracy for a system in which multipath is not a consideration.

On the other hand, if the multipath model adopted is valid, there are indications that 94 GHz will not provide adequate angle tracking error over typical types expected to be encountered in tactical operations in adverse environments. If the trend of these calculations is consistent with projected performance from realistic terrain models, operation at 220 GHz may also be necessary to insure an adequate accuracy for missile impact over the desired clear weather range of 3 km. If this is the case, a reduced low visibility operating range will be incurred. Thus, among the trade-offs to be considered will be that of adequate clear weather operation against maximum range of low visibility operation. A 94 GHz system, for example, might perform reasonably well over a 1.5 - 2 km range interval in a wide range of adverse meteorological and terrain conditions, whereas a 220 GHz system might extend the clear weather operating range to 2.5 - 3 km while restricting the adverse

weather range to < 1.5 km.

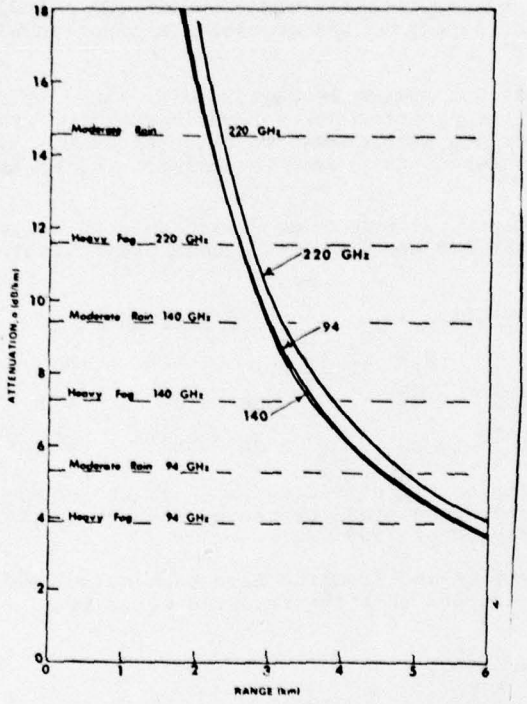

Figure 16. Projected performance levels for acquisition under different weather conditions for a 1 kW source. The conditions are: moderate rain 4 mm/hr, 80°F; heavy fog, 30 m visibility, 40°F.

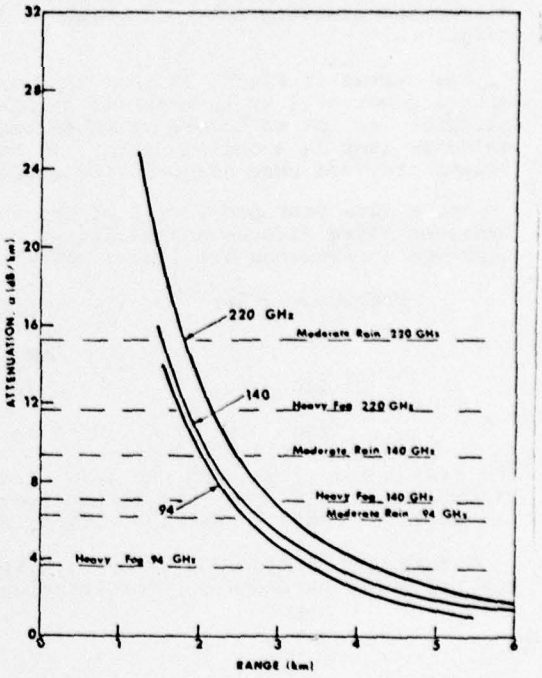

Figure 17. Projected performance levels for tracking under different weather conditions. The conditions are the same as those given in Figure 16.

Preliminary system studies have shown that millimeter guidance systems offer a potentially significant improvement in penetration of adverse environments which limit the visibility of electro-optical guidance systems. Further, there is the potential for improved accuracy with adequate penetration under adverse environmental conditions when compared to guidance systems operating in the microwave frequency band.

The state-of-the-art will currently support the development of operational breadboard beamrider or command guidance systems at 94 or 140 GHz. One such breadboard system has been developed at BRL[20], and tests performed at both BRL and MIRADCOM on tracking and guidance link operational simulations were found to be supportive of this millimeter guidance concept. MIRADCOM is also supporting several contractor-developed millimeter guidance systems which will involve development and testing of both differential guidance and beamrider concepts. As a part of these efforts, the evolutionary development of critical subsystems such as the tracking radar and guidance link will provide a means for performing operational tests to determine multipath effects, measure target signatures, and assess various schemes which have been proposed for missile capture; however, a very significant concern is the development of an appropriate target acquisition concept for an autonomous millimeter guidance system, and this and other critical technology issues are addressed in Table 9.

A basic deficiency in the current millimeter technology base is the lack of measured target, terrain and atmospheric data. Without these data, accurate quantitative estimates of system performance in realistic tactical environments cannot be made with any degree of confidence. Thus, the development of millimeter measurement systems operating in the windows at 94, 140 and 220 GHz is a critical step in establishing their operational limitations in terms of meteorological conditions and reduced visibility situations resulting from smokes and other battlefield-generated aerosols. The acquisition of these data should be a major part of a program to develop millimeter guidance systems.

Table 9. Critical Beamrider Technology Areas

ACTIVITY	RATIONALE	RESOURCES NEEDED
Multipath	Limits tracking accuracy; Degrades beam/guidance	mm λ radar/optical tracker; field problems - frequency and terrain dependence
Wavelength Selection	Potential of improved tracking vs λ; source and detector performance dependence; multipath dependence; optimum search/acquisition wavelength	Transmitter/receivers; accurate propagation measurements in smoke, rain, fog and high humidity; supporting meteorological measurements
Target Signatures	Reduce angle error and signal loss	Transmitters/receivers; Signal Processing; Pulse-to-Pulse target reflectivity data; function of target aspect
Target Acquisition	Prime system function	Coherent system measurements to feed computer simulation to determine signal processing required, e.g. MTI, vibrational signatures, and
Capture	Required for initiation of missile guidance	Determine required beam profile vs range for capture; near field measurement; determine concepts for multifunctional capture/track/guidance
Acceleration Hardened Schottky Diodes	Required for missile receiver	Trade-off video/superheterodyne for missile receivers; test diodes under shock, simulated flight conditions
Near mm wave Components	Required for low loss system	Quasi-Optical approach - circulators, isolators, modulators, antenna conscan schemes, diplexers, rotary joints, mixers, local oscillators
Transmitters	High Power Stable Sources Required	EIO's vs Impatts; develop stability techniques; chirp techniques; gyrotrons - long term source
Target Tracking Techniques	Need to provide high accuracy target coordinates and maintain good pointing accuracy	High precision tracking radar-spread spectrum techniques for decorrelation of target scatterers; coherent, frequency agile system
Clutter Characteristics	Information required for enhancement of target-to-clutter signals	Measurements of NMMW clutter characteristics terrain masking effects; establish discrimination schemes

Comments on other systems applications

The above discussion of the beamrider indicates some of the factors which can influence the design and operation of a NMMW system. The same type of considerations must be made for other potential NMMW systems. Only brief comments can be made here on some of these systems.

Target designator and semi-active seekers

Target designators have been successfully operated at 1.06 μm in clear atmosphere. However, during adverse propagation conditions (mainly fog and smoke), the IR designators are ineffective. The existing IR systems, operating at 1.06 μm, have the advantage of having all laser power incident upon the target. This is important since the reflectivity of terrain and vegetation exceeds that of the target at 1.06 μm. For NMM wavelengths, two techniques have been investigated[3]: the case in which the target fills the beam and the more general case for long wavelengths in which the beam size exceeds the target dimensions. Because target reflectivity is expected to exceed background reflectivity, a largest pulse logic is postulated for designation of the target in clutter.

Command guidance

The application of NMMW command guidance to anti-helicopter or anti-aircraft missions appears to be feasible. Command guidance is also applicable in a ground-to-ground anti-armor role, but no clear advantage over Beamrider guidance is evident at this time. The technology barriers associated with this guidance concept are similar to those for the Beamrider, and the general conclusions reached for the beamrider guidance concept apply to command guidance. The state-of-the-art can support breadboard system development at 94 and 140 GHz, and additionally, the window at 220 GHz appears to be applicable if source development evolves as projected by current technology.

Target surveillance and acquisition

For the successful operation of battlefield NMMW systems, it is important that target acquisition and surveillance techniques be applicable to NMMW systems. This would provide autonomous operation. For the optimum weapon system, several combinations of different wavelength sub-systems must be evaluated to obtain the optimum combination of surveillance,

acquisition, and guidance. Among the systems that have been identified as potential NMMW applications are:

battlefield ground-to-ground target acquisition;
airborne surveillance by RPV radars of land-based targets;
long-range surveillance and target acquisition;
target acquisition for NMMW airborne missile seeker systems;
horizon search radars;
shipboard surveillance radars;
track-while-scan systems for short-range self-defense systems (point defense);
restricted scan target acquisition for missile systems.

A large number of equipment and technique developments are necessary to ascertain the applicability of NMM waves. Techniques for search, recognition and classification have been identified [3] but more detailed investigations are needed to implement these techniques. Greater transmitter power, improved receiver sensitivity, new low-loss components and light-weight rapid-scan antennas are necessary. Source stability for coherent operation must be greatly improved. For implementation of the recognition/classification techniques, target characteristics, clutter effects and atmospheric effects are among the phenomenology that must be thoroughly documented.

Boost phase plume detection

Calculations have been performed to determine the feasibility of detecting missile plumes during the boost phase of the vehicle [22]. In the altitude regime of 30-100 km, it has been shown that, for a solid propellant system, molecular species, e. g. H_2O and H Cl, emit to permit radiometric detection from aircraft or satellites. Airborne radiometric observations are required to confirm predictions. The necessary passive technology is developing but must be extended to wavelengths as short as ~350 μm. Independent analysis of the bus stage indicate that spectral line opacity is sufficiently high to be detectable in occultation against the earth's radiation.

Conclusions

From the studies which have been performed, it can be concluded that the NMMW region offers a compromise for good resolution under adverse propagation conditions. Most systems, which have been investigated, profit from the narrow antenna beams available at NMM wavelengths, but are limited by atmospheric conditions. In some cases, the range limitations imposed by the atmosphere serve as an advantage for convert operation.

In order to utilize the NMMW spectral region properly, considerable technology must be developed. High-power sources, low loss components, precision antennas, sensitive receivers and stable local oscillators are priority devices to allow systems operations to be performed at NMM wavelengths. For many systems, highly coherent transmitters are required. This necessitates development of phase-locking and injection-locking technology for high-power sources. A driving force in extending military operation to NMM wavelengths is the prospect of small-size systems where space and antenna apertures are limited. Low cost, which is not a current characteristic of NMMW components, is expected to be an ultimate achievable goal.

One cannot expect to achieve everything that a system demands by employing NMM waves, and those working in the field are not doing this. Phenomenology in the form of atmospheric, terrain/clutter, target, and materials characteristics must be thoroughly developed for comparison with operation at other wavelengths. Thus far, studies have estimated certain characteristics and projected reasonable operational parameters for devices. From the considerations that have been made, optimum operation can be expected from hybrid IR/NMMW systems which will utilize the best of both spectral regions.

This work has been sponsored in part by the Harry Diamond Laboratories through the Army Research Office Contract No. DAAG29-77-C-0026.

References

1. 1974 Millimeter Wavelength Technical Conference, NELC/TD 308 Naval Electronics Laboratory Center, San Diego, CA 26-28, March 1974;

Proceedings of the DARPA/Tri-Service Millimeter Wave Conferences (8), Defense Advanced Research Projects Agency, Arlington, VA 22209

2. J. J. Gallagher, M. D. Blue, R. G. Shackelford, "Applications of Extreme Infrared to Missile Systems", Final Report on Basic Agreement DAHC04-72-A0001, Task Order 76-8, Battelle Columbus Laboratories, January, 1976;

L. D. Strom, "Applications for Millimeter Radars", System Planning Corporation, Report No. 108, Contract No. DNA001-73-C-0098, ARPA Order No. 2353, December, 1973 AD529566;

"Low Probability of Intercept Multifunctional Tactical Sensors", Final Report, Contract F33615-76-C-1227, Raytheon Company, January, 1978;

Paul W. Kruse and Vitalij Garber, "Technology for Battlefield Target Recognition in Inclement Weather", Proceedings of the 23rd Annual IRIS Conference, 1976;

K. L. Koester, "Millimeter Wave Propagation", Norden Div. of United Technologies, Report 4392R005, 1972 (U);

A. M. Peterson, et al, "Low Angle Radar Tracking", Stanford Research Inst. Tech. Rept. JSR 74-7(U) February 1976, pages 53-57, 97-98;

J. J. Gallagher et al, "Applications of Submillimeter Wave Gigawatt Sources", Ga. Inst. of Technology, Engr. Experiment Station, Report GT/EES Project A-1717, DARPA Order 2840, 1975 (U);

R. LeLevier, "Applications of High Power Microwave/Millimeter Wave Technology" (U), R. and D Associates, Strategic Technology Final Report RDA-TR-4600-018, July 1975 (Report Secret);

Victor W. Richard, "Millimeter Wave Radar Applications to Weapons Systems", Ballistic Research Laboratories Memorandum Report No. 2631, June 1976 (U);

K. Evans, J. Dooley, R. Haraway, and H. Green, "Applications of Millimeter Wave Technology to Antiarmor Weapons Systems", Technical Report C-77-6, 22 February, 1977, U. S. Army Missile Research and Development Command, Redstone Arsenal, Alabama 35809

3. R. K. Parker, T. F. Godlove, and V. L. Granatstein, "Applications of High Power Microwave Sources - A Panel Study" (U), Vol. 1. NRL Memorandum Report 3339 (1976) (Report Secret);

"Interim Report on the Ad Hoc Study Group on the Military Applications of Millimeter Waves" Nato Document AC/243-D/332, AC/243(Panel III)D/115, June 1974 (U);

S. M. Kulpa and E. A. Brown, "DARCOM/DARPA Near-Millimeter Wave Technology Base Study", Harry Diamond Laboratories (1979);

4. S. M. Kulpa and E. A. Brown, "Propagation and Target/Background Characteristics", Volume 1 of Near-Millimeter Wave Technology Base Study, Harry Diamond Laboratories, October, 1979;

5. J. Preissner, "The Influence of the Atmosphere on Passive Radiometric Measurements", AGARD Conference Proceedings No. 245, Millimeter and Submillimeter Wave Propagation and Circuits, edited by E. Spitz, pp. 48-1 to 48-14, 4-8 September, 1978;

6. N. E. Feldman and S. J. Dudzinsky, Jr., "A New Approach to Millimeter-Wave Communications", R-1936-RC, April, 1977;

7. J. J. Gallagher, G. Loefer, J. L. Edwards, and J. P. Burns, "Microwave Instrumentation Applied to Aerosols and Smokes", Final Report, Contract No. DAA15-76-C-0087, 7 January 1979;

R. W. McMillan, R. Rogers, R. Platt, D. Guillory, J. J. Gallagher, and D. E. Snider, "Millimeter Wave Propagation through Battlefield Dust", Final Report, ASL-CR-79-0026-1, Contract DAAG29-77-C-0026, June, 1979;

J. J. Gallagher, R. C. Rogers, O. A. Simpson and J. H. Rainwater, "Millimeter Wave Propagation Through Smokes", Final Report, Contract No. DAAA11-77-C-0099, October, 1979;

8. G. D. Lukes, "Penetrability of Haze, Fog, Clouds and Precipitation by Radiant Energy Over the Spectral Range 0.1 Micron to 10 Centimeters", Naval Warfare Analysis Group of the Center for Naval Analysis, Study No. 61, under Contract N00014-68-A-0091, November, 1968;

9. H. J. Aufm Kampe, "Visibility and Liquid Water Content in Clouds in the Free Atmosphere", Journ. of Met 1, 54 (1970)

10. D. Deirmendjian, "Scattering and Polarization Properties of Water Clouds and Hazes in the Visible and Infrared", Applied Optics 3 , #2, 187-196, February 1964.

11. V. W. Richards and J. E. Kammerer, "Rain Backscatter Measurements and Theory at Millimeter Wavelengths", Ballistic Research Laboratories, Report No. 1838, October 1975.

12. See Reference 5.

13. N. A. Armand, A. O. Izyumov, and A. V. Sokolov, "Fluctuations of Submillimeter Waves in a Turbulent Atmosphere", Radio Engineering and Electronics Physics 16, 8, 1259 (August, 1971)

14. D. E. Snider, J. C. Wiltse, and R. W. McMillan, "The Effects of Atmospheric Turbulence and Adverse Weather on Near-Ground 94 and 140 GHz Systems", Workshop on Millimeter and Submillimeter Atmospheric Systems, Redstone Arsenal, Alabama, March, 1979.

15. J. H. Van Vleck and V. F. Weisskopf, Rev. Mod. Phys. 17, 227 (1945)

16. E. P. Gross, "Shape of Collision-broadened Spectral Line", Phys. Rev. 97, 394 (1955)

17. N. E. Gaut and E. C. Reifenstein, III, Environmental Research and Technology Report No. 13, NASA Contract NAS8-26275, Waltham, MA

18. R. A. Bohlander, et al, "Excess Absorption by Water Vapor and Comparison with Theoretical Dimer Absorption", D. T. Llewellyn-Jones, "Laboratory Measurements of Absorption by Water Vapor in the Frequency Range 100-1000 GHz", and H. A. Gebbie, "Observations of Anomalous Absorption in the Atmosphere", Proceedings of the Workshop on Atmospheric Water Vapor, Vail, Colorado, 11-13 September, 1979 (Institute for Atmospheric Optics and Remote Sensing, Hampton, Virginia 23666)

19. A. H. Green and F. King, "Preliminary Millimeter Beamrider Feasibility Assessment", Internal Technical Note RE-77-3, Advanced Sensors Directorate, U. S. Army Missile Research, Development and Engineering Laboratory, U. S. Army Missile Command, Redstone Arsenal, 1 October, 1976.

20. D. G. Bauerle, R. A. McGee, J. E. Knox and H. B. Wallace, "140 GHz Beamrider Feasibility Experiment", Interim Memorandum Report No. 538, Ballistic Research Laboratories, January, 1977.

21. R. G. Shackelford and J. J. Gallagher, "Millimeter Wave Beamrider System", Advanced Sensors Directorate, U. S. Army Missile Research and Development Command, Technical Report TE-CR-77-7, August, 1977.

22. J. J. Gallagher, P. B. Reinhart, R. W. McMillan and J. H. Rainwater, "The Investigation of the Feasibility of Airborne Detection of Submillimeter Missile Plume Radiation", Final Report, Contract No. DASG60-78-C-0031 (February 22, 1979).